

Accepted Manuscript

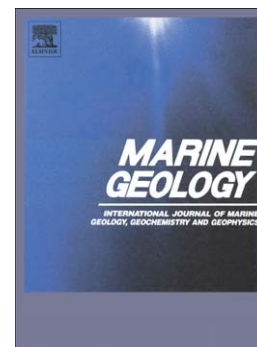
Sedimentology of Seismo-Turbidites off the Cascadia and Northern California
Active Tectonic Continental Margins, Northwest Pacific Ocean

Julia Gutiérrez-Pastor, C. Hans Nelson, Chris Goldfinger, Carlota Escutia

PII: S0025-3227(12)00283-6
DOI: doi: [10.1016/j.margeo.2012.11.010](https://doi.org/10.1016/j.margeo.2012.11.010)
Reference: MARGO 4862

To appear in: *Marine Geology*

Received date: 25 September 2011
Revised date: 26 November 2012
Accepted date: 28 November 2012



Please cite this article as: Gutiérrez-Pastor, Julia, Nelson, C. Hans, Goldfinger, Chris, Escutia, Carlota, Sedimentology of Seismo-Turbidites off the Cascadia and Northern California Active Tectonic Continental Margins, Northwest Pacific Ocean, *Marine Geology* (2012), doi: [10.1016/j.margeo.2012.11.010](https://doi.org/10.1016/j.margeo.2012.11.010)

This is a PDF file of an unedited manuscript that has been accepted for publication. As a service to our customers we are providing this early version of the manuscript. The manuscript will undergo copyediting, typesetting, and review of the resulting proof before it is published in its final form. Please note that during the production process errors may be discovered which could affect the content, and all legal disclaimers that apply to the journal pertain.

Sedimentology of Seismo-Turbidites off the Cascadia and Northern California Active Tectonic Continental Margins, Northwest Pacific Ocean

Julia Gutiérrez-Pastor¹, C. Hans Nelson¹, Chris Goldfinger², Carlota Escutia¹

¹*Instituto Andaluz de Ciencias de la Tierra (IACT) CSIC-UGR*

Avda. de Las Palmeras nº 4, 18100. Armilla, Granada, Spain, juliagp@ugr.es

²*Oregon State University, College of Oceanic and Atmospheric Sciences*

104 Ocean Admin. Bldg., Corvallis OR 97331, USA.

.....

Abstract

Holocene turbidites from turbidite channel systems along the active tectonic continental margins of the Cascadia Subduction Zone (offshore Vancouver Island to Mendocino Triple Junction) and the northern San Andreas Transform Fault (the Triple Junction to San Francisco Bay), have been analyzed for sedimentologic features related to their seismic origin. Centimeter thick silt/sand beds (turbidite base) capped by mud layers (turbidite tail) and interbedded with hemipelagic silty clay intervals with high biogenic content have been characterized by visual core descriptions, grain-size analysis, x-ray radiographs and physical properties.

Along the northern California margin in upstream single tributary canyons and channels, most turbidites are uni-pulsed (classic fining up) whereas downstream below multiple tributary canyon and channel confluences, most deposits are stacked turbidites. Because each set of stacked turbidites has no hemipelagic sediment between each turbidite unit and each unit has a distinct mineralogy from a different tributary canyon, we interpret that a stacked turbidite is

deposited by several coeval turbidity currents fed by multiple tributary canyons and channels with synchronous triggering from a single San Andreas Fault earthquake.

The Cascadia margin is characterized by individual multi-pulsed turbidites that contain multiple coarse-grained sub-units without hemipelagic sediment between pulses. Because the number and character of multiple coarse-grained pulses for each correlative multi-pulsed turbidite is almost always constant both upstream and downstream in different channel systems for 600 km along the margin, we interpret that the earthquake shaking or aftershock signature is usually preserved, for the much stronger Cascadia (≥ 9 Mw) compared to weaker California (≥ 8 Mw) earthquakes, which result in upstream uni-pulsed turbidites and downstream stacked turbidites. Consequently, both the strongest (≥ 9 Mw) great earthquakes and downstream confluences cause multi-pulsed and stacked turbidites that are typical for seismo-turbidites generated by a single great earthquake. Along both margins, earthquake triggering and multi-pulsed or stacked turbidites become an alternative explanation for amalgamated turbidite beds in active tectonic margins and show that multiple grain-size pulses and reverse grading are not unique criteria for hyperpycnites, thalweg levee turbidites, or mini-basin margin turbidites.

The analyses of the turbidites along the Cascadia and northern California margins reveal common sedimentologic characteristics of turbidites triggered by great earthquakes that can be used to distinguish seismo-turbidites in other active tectonic margins around the world.

Keywords: seismo-turbidite, sedimentology, earthquakes, Cascadia Subduction Zone, San Andreas Fault, continental margins

1. INTRODUCTION

Marine and onshore paleoseismic records are being studied along the Cascadia subduction zone margin and northern California transform fault margin (Figs. 1, 2). Great earthquakes (≥ 8

Mw) from the Cascadia subduction zone have generated paleoseismic turbidites offshore and tsunami sands and co-seismic subsidence buried marshes onshore (Atwater, 1987; Adams, 1990; Darienzo and Peterson, 1990; Atwater et al., 1995; Atwater and Hemphill-Haley, 1997; Nelson et al., 1995, 2000; Satake et al., 1996, 2003; Kelsey et al., 2002; Goldfinger et al., 2003a, 2003b).

The northern California margin, associated with the active San Andreas Fault, also has offshore and onshore paleoseismic record based on the geodetic data and fault offset history (Prentice, 1999; Niemi and Hall, 1992; Schwartz et al., 1998; Knudsen et al., 2002; Segall, 2002; d'Alessio et al., 2005; Kelson et al., 2006; Zhang, et al., 2006).

Along offshore margins, the paleoseismic record includes turbidites in canyon and basin floor channel turbidite systems (Goldfinger et al., 2007, 2008). Because both Cascadia and northern California margins have recorded a Holocene history of turbidites mainly triggered by great earthquakes, they are ideal places to develop a turbidite sedimentologic model to characterize their seismic triggering. Until now in these margins the turbidite studies have been focused on the correlation of turbidites triggered by earthquakes based on stratigraphic datums (Adams, 1990; Nelson et al., 2000), AMS radiocarbon ages, physical properties (Goldfinger et al., 2003a, 2003b, 2006, 2007, 2008) and recurrence time intervals determined by hemipelagic sediment thickness and sedimentation rates (Gutierrez-Pastor et al., 2009). In this paper we analyze the detailed sedimentologic characteristics of turbidites from Cascadia and northern California margins by using a wide variety of analyses. Several authors in other areas have attempted to define sedimentologic differences between turbidites triggered by earthquakes and turbidites triggered by other mechanisms (Gorsline et al., 2000; Nakajima and Kanai, 2000; Shiki et al., 2000, Strasser et al., 2006). In this paper, we add further observations to characterize turbidites generated by great earthquakes, for which we use the term seismo-turbidites.

We investigate the sediment using visual core descriptions, photos, x-ray imagery, quantitative grain size analyses, mineralogical analysis and physical properties of high-resolution magnetic susceptibility and density. For our turbidite characterization, we examine

representative sedimentologic features of turbidites from tributary source channels and below their confluences. Although we realize that some literature calls surges of turbidity currents pulses, we define coarser-grained sub-units of individual turbidites from these surges as pulses, to be consistent with our previous publications (e.g. Goldfinger et al., 2003a, 2008, 2012, Gutierrez Pastor et al, 2009). Using this terminology for seismo-turbidites, we describe “unipulsed” (single fining up turbidites), and “multi-pulsed turbidites (individual turbidites with multiple coarse-grained pulses). We also encounter “stacked turbidites” (multiple coarse-grained turbidite beds with no intervening hemipelagic sediment) (e.g. Strasser et al., 2006). Stacked turbidites deposit below tributary canyon/channel confluences from coeval turbidity currents, which are synchronously triggered by the same earthquake.

Finally, we propose a sedimentologic model in space and time for these types of seismo-turbidites that provides information about the triggering, source, mechanisms of deposition and even relative magnitude of earthquakes. This postulated model may help to define and understand seismo-turbidite deposition in other active tectonic margins.

2. GEOLOGICAL SETTING AND TURBIDITE SYSTEMS

2.1. Cascadia Continental Margin

The Cascadia continental margin overlies the subduction zone of the Gorda and Juan de Fuca plates thrusting beneath the North American plate (Fig. 1). Cascadia Basin is the abyssal seafloor off northern California, Oregon, Washington, and Vancouver Island along the subduction zone. A wide variety of modern turbidite systems (e.g. submarine fans, deep-sea channel, apron) all containing correlative, synchronously triggered turbidites are found in the Cascadia Basin (Fig. 1) (Nelson et al., 2000). Cascadia Channel is a deep-sea channel system fed by multiple tributary canyons, and extends for hundreds of kilometers across Cascadia Basin. For our detailed sedimentologic analysis, we have selected well correlated turbidites within the Juan de Fuca Channel that is a tributary channel to the Cascadia Channel (Fig. 1).

2.2. Northern California Continental Margin

Along the continental margin of northern California, the San Andreas Fault extends from San Francisco, where the fault parallels the coast and then further north underlies the margin and Noyo Canyon until the Mendocino Triple Junction (Fig. 2). Along the northern California margin there are numerous canyon/channel systems containing earthquake-triggered synchronous Holocene turbidites (Goldfinger et al., 2003a, 2003b, 2007, 2008)

From the north, beginning at Cape Mendocino, to the south at Monterey Bay, the canyons and channels are: Gorda, Viscaino, Noyo, Arena, Gualala, Albion, Bodega Cordell, Farallon, Montara, Pioneer and Monterey (Fig. 2) (Goldfinger et al., 2003a). The turbidite channels join together creating downstream confluence pathways. Noyo Channel, which is found south of Cape Mendocino, extends seaward for more than 200 km from the mouth of the canyon where it has a confluence with Viscaino and Gualala Channels (Fig. 2). Southern Point Arena and Gualala canyons join at the base of the continental slope to form a channel that extends 100 km until its confluence with Noyo and Viscaino Channels. Similarly, north of the Noyo Channel, the Viscaino channel is formed by multiple tributaries that meet to develop the main channel traveling more than 200 km until a confluence with Noyo, Gualala and Cordell. For our sedimentologic characterization, we have selected turbidites from the Noyo, Gualala and channels downstream from confluences to examine representative turbidites from tributary source channels and below their confluence.

3. SEDIMENT ANALYSIS METHODS

During 1999 and 2002 cruises for paleoseismic studies, cores were recovered from all the turbidite systems along the Cascadia and northern California margins. The core locations were selected carefully in channel pathways integrating all available swath bathymetry and archive cores in a GIS data base. This allowed exploring in real time the ocean floor and channel

systems using bathymetry, backscatter data, and interactive fly-troughs of the channel morphology. Core sites were chosen to take advantage of known depositional segments of channels versus non-deposition or erosional segments to capture the most complete turbidite record.

In Cascadia Basin the Oregon State University wide diameter (10 cm) coring gear was employed to collect 44 piston cores of 6-8 m length and 44 companion trigger cores (also 10 cm) of 2 m length, as well as seven box cores of 0.5 m length x 0.5 m width. On the northern California margin, 69 piston/trigger pairs and 10 jumbo Kasten cores (of 3 m length x 20 cm width) were collected in 2002. On board the ship, turbidites versus hemipelagic sediment were logged by visual core lithologic analysis (Fig. 3A). Color photos of each core were taken to complement the visual core observations. Analysis of the sand fraction (> 62 microns) of the hemipelagic sediment using a binocular microscope was done to determine the micro fauna content (foraminifera and radiolaria), main lithology of the sand grains, plants fragments and micas. This analysis was done to distinguish the hemipelagic sediment from the turbidite tail and also to determine the Holocene/Pleistocene boundary. In addition, hemipelagic sediment thickness was measured to calculate accurate sedimentation rates for estimation of turbidite recurrence time intervals (Gutierrez-Pastor et al., 2009)

To help the turbidite identification, while at sea, a Geotek Multisensor Core Logger (MSCL) was used to obtain continuous measurements of physical properties (density (g/cm³), p-wave velocity and magnetic susceptibility (MST) for each core (Figs. 3B, 3C). Onland, high-resolution magnetic susceptibility data (SI) were collected from each core using a point probe (Bartington MS2E high-resolution surface sensor) at 1 cm and 3 mm intervals. The physical property measurements have been very useful as proxies for grain size to identify individual turbidites with multiple sandy/silty multiple coarse-grained units (pulses) without hemipelagic sediment in between the pulses (see Goldfinger et al., 2007, 2008). A semi-quantitative mineralogical analysis was done with smear slides from critical turbidites to identify the Mazama Ash content (Mazama Ash Datum: 7627 \pm 150 cal yr B.P., e.g. Zdanowicz et al., 1999) in the Cascadia margin and the sand/silt mineral provenances of tributary canyons in the

northern California margin. Between two to three centimeters of hemipelagic sediment were sampled below the base of each turbidite bed to obtain planktonic foraminifera for radiocarbon ages (Fig. 3A). Ages were obtained from foraminifera using Accelerator Mass Spectrometry (AMS) methods at the Lawrence Livermore Laboratory. X-ray radiographs were taken in many cores from both margins to show grading and internal sedimentary structures of the light-colored turbidite sand/silt beds and to distinguish the darker intensity hemipelagic sediment from the turbidite tail mud (Fig. 3B). Grain size analyses for selected turbidites from both Cascadia and Northern California margins were performed with a electro-resistance multichannel particle-size analyzers (EMPSA), manufactured by Coulter Counter (<http://pubs.usgs.gov/of/2000/of00-358/text/chapter1.htm>) (Blott and Pye, 2006). With this method we have measured the size distribution of particles in the range of 0.4 microns to 850 microns. Prior to the measurements, we treated the ~ 10 g samples with hydrogen peroxide to remove the organic matter. The results are shown in granulometric curves that reflect the variations of grain size in each part of the individual turbidites. The grain size analyses were done to distinguish individual turbidites with complex multiple pulses of coarser grain size from turbidites with simple fining upward gradation, and to identify the different parts of the turbidite (base, turbidite body and tail) and the hemipelagic sediment just below the turbidite base. Also, we wanted to recognize associated grain size patterns in turbidites triggered by earthquakes compared with turbidites triggered by other mechanisms.

Broad mineral provenance bins were determined from standard heavy-mineral analysis techniques (Goldfinger et al., 2007). We sieved the sand fraction from selected turbidites, and separated the heavy minerals with tetrabromoethane (specific gravity is 2.9), separating light and heavy fractions. The grain mounts of the heavy minerals were then counted for at least 300 grains, 200 being true heavy minerals. All the physical property logs, X-ray radiographs, lithologic log data, together with mineralogical and grain size analyses have been integrated to compare the sedimentologic characteristics of the turbidites.

4. PALEOSEISMIC TURBIDITE RECORD: PREVIOUS RESULTS

Along the Cascadia and northern California margins, turbidites have been recognized in our cores collected in 1999, 2002 and in archive cores (Nelson, 1968, 1976; Griggs, 1969; Duncan et al., 1970). For the past 50 years, studies of hundreds of cores with thousands of grain size analyses of sand/coarse silt beds, and the density and magnetic susceptibility logs which this study shows are proxies for grain size, all show graded turbidite beds (Figs. 3, 4) (e.g. Nelson, 1968, 1976; Griggs, 1969; Duncan et al., 1970; Nelson et al., 2000; Goldfinger et al., 2008, 2012). The individual turbidites exhibit sharp bases and contain one simple fining up or multiple fining up coarse-grained pulses of sand and/or silt a few centimeters thick. Turbidite bases are overlain by a sediment that is composed of a bioturbated interval of mud (silt and clay), resulting from the deposition of the tail of the turbidity-current flow.

Turbidites are emplaced over the hemipelagic sediment that is composed of bioturbated clay with a coarse fraction ($>62\mu$) of dominant microfauna tests (foraminifera and radiolaria) in distal sites, and with more abundant terrigenous sediment (up to 50%), such as plant fragments and micas, and less abundant microfauna (less than 50%) in proximal sites near the base of the continental slope (Fig. 3A) (Nelson, 1976). Following the techniques of Nelson (1968, 1976), when the boundary between turbidite and hemipelagic sediment was difficult to differentiate visually, we sampled the sand fraction of the sediment above and below the inferred boundary and counted microfossils and terrigenous grains with a binocular microscope (Fig. 3A). Once the hemipelagic sediment was identified by the dominance of planktonic tests, the number of foraminifera (dominance = Pleistocene) and radiolarians (dominance = Holocene) were counted.

Along the Cascadia margin, Holocene turbidites have been deposited synchronously in different channels and aprons separated by hundreds of kilometers, when turbidite deposition was not expected because the continental shelf is wider during high sea levels and the canyon heads are further from the shoreline sediment source. Great earthquakes on the subduction zone are the best candidate to explain the synchronicity of turbidite triggering in such a wide area

and variety of different turbidite systems during the Holocene time (Adams, 1990; Nelson, et al., 2000; Goldfinger et al., 2003a, 2003b).

To show synchronicity of turbidite triggering by earthquakes, the confluence test postulated by Adams (1990) utilizes the first occurrence of Mazama ash (7627 ± 150 cal yr B.P) (Zdanowicz et al., 1999) in a turbidite as a marker bed; synchronous triggering is shown when the number of upstream post-Mazama ash (MA) turbidites in multiple tributaries equals the number of post (MA) turbidites downstream below the tributary confluences. If the turbidites were triggered by non-synchronous random events in the tributaries, the number of turbidites below tributary canyon/channel confluences would be additive and many more than the 13 post MA turbidites observed both upstream and downstream from confluences. In Cascadia Basin, both the Juan de Fuca and other tributary channels and the Cascadia Channel below the confluence contain 13 post-MA turbidites (Fig. 1) (Adams, 1990; Nelson et al., 2000). This test is supported by turbidite correlations based on ^{14}C ages and correlative physical properties between sample sites that are separated by several hundred kilometers along the Cascadia margin (Figs. 1, 3C) (Goldfinger et al., 2008, 2012).

We have extended the correlation of turbidites below the T13 post MA turbidites so that a total of 19 Holocene turbidites can be correlated in northern Cascadia Basin (Goldfinger et al., 2008, 2012). To help extend the correlation in time, the Holocene/Pleistocene boundary has been determined by the dominance of radiolaria in the Holocene versus the dominance of foraminifera sediment in the Pleistocene sediment and by a clear change in the sediment color (Nelson, 1968; Duncan et al., 1970; Nelson, 1976; Gutierrez-Pastor et al., 2009).

The northern California margin also has a turbidite paleoseismic history even though no good datum such as the Mazama Ash or color and sediment compositional change of Pleistocene to Holocene hemipelagic sediment has been found (Goldfinger et al., 2003a, 2003b, 2007; Gutierrez-Pastor et al., 2009). In our previous research we have observed that along the northern California margin, turbidites exhibit uni-pulsed or apparent multi-pulsed coarse silt or sand bases of several centimeters and a muddy tail.

In the northern California margin, Noyo Channel has been studied in detail because its Noyo Canyon source is offset by the San Andreas Fault and thus sedimentary processes are affected directly by earthquakes associated with the canyon (Fig. 2). The channel also has an expanded Holocene turbidite record recovered from five cores containing 2-25 turbidites that can be correlated along strike (Fig. 2) (Goldfinger et al., 2007). In the Noyo Channel, as in other turbidite channels of the northern California margin, correlations have been based mainly on ¹⁴C ages, heavy mineralogy and stratigraphic correlation with physical property proxies. Examples are shown in figures 3B and 3C for the northern California and Cascadia margins respectively (Goldfinger et al., 2003a, 2003b, 2007, 2008, Gutierrez-Pastor et al., 2009).

In previous papers, we have discussed the merits of other possible triggers for turbidity current generation such as storm wave loading, tsunamis, sediment loading, hyperpycnal flow and aseismic accretionary wedge slip, but conclude that the evidence supports seismic triggering (Nelson et al., 2000; Goldfinger et al., 2003a, 2003b, 2006, 2007, 2008, 2012)

5. RESULTS: SEDIMENTOLOGIC CHARACTERIZATION OF TURBIDITES

5.1. Cascadia Margin.

To characterize turbidites we have selected one correlative turbidite from two different turbidite channels: 1) the tributary Juan the Fuca Channel in a proximal location of northern Cascadia Basin and 2) the Cascadia Channel in a downstream distal site below a confluence of this channel and another proximal tributary channel to the Cascadia Channel, the Willapa Channel (Fig. 1). The samples consist of turbidite number 3 (T3) of Piston core (PC) 12 in Juan de Fuca Channel, T3 of 25PC in Cascadia Channel and another turbidite of 14PC in Willapa Channel (Fig. 4). Our goal is to see how the sedimentologic features in the same correlative turbidite vary from proximal to distal in a channel and downstream from a confluence of several tributary canyons or channels.

5.1.1. T3 in Juan de Fuca Channel

For the descriptions, turbidites have been separated into a coarse-grained base, a muddy turbidite tail and hemipelagic sediment above. To characterize our Juan de Fuca and Cascadia Channel turbidites, we use the term “pulse” for the coarse grained sediment part of a turbidite. The Juan de Fuca/Cascadia channel turbidites can be uni- or multi-pulsed with more than one coarse-grained sub-unit in an individual turbidite. See also the last two paragraphs of the introduction for clarification of the pulse terminology. Visual core observations suggest that T3 in Juan de Fuca Channel of 12PC has a sand/silt thickness of 9 cm with two pulses shown by the magnetic log compared with the one fining-up pulse shown by the grain size and density log, a muddy tail of 5 cm and hemipelagic sediment below of 5 cm, as shown by the darker homogeneous color of the X-ray, lighter lithologic color of the sediment, and the coarse fraction analysis that has been done below each turbidite base (Fig. 3A). The X-ray radiograph shows a light intensity of the X-ray for the silt lamina that coincide with the highest value peak in the density and magnetic log signatures for the coarse silt base of the turbidite (Fig. 4). This is a fine-grained turbidite as described by Piper and Deptuck (1997) with the typical fining upward of grain size (Tables 1A, 1B) (Bouma, 1962). Grain size distribution curves have been calculated for each sample representing the % and cumulative % of grain sizes in volume (Table 1; Appendix 1A). The T3 appears as a uni-pulsed fining up turbidite with d50 between medium and fine silt. The largest grain size transported by the turbidity current (d90) is very fine sand (Table 1B). In the base of T3, silt lamina at 34.5 cm are represented by a curve mode going to the right toward coarser values and by the high content of silt (63%) and sand (21%) (Table 1B; Appendix 1A). Curves representing samples at 31.5 and 30 cm show broader mode distribution with a progressive decrease in the sand content and also with a progressive increase in the silt/clay content. Almost the same median grain size at 30 cm (6.5 ϕ) compared with 31.5 cm (6.3 ϕ) shows that the second peak in the magnetic log signature does not represent coarse grain size.

5.1.2. *Turbidite 3 in Cascadia Channel*

In Cascadia Channel T3 from core 25PC can be divided into two main intervals, the first one from ~109 cm to ~ 97 cm that is composed of three sandy/silty pulses at 109-108 cm, 105-104 cm and 101-97 cm, and the second interval from 97 cm to 52 cm that is composed of dark turbidite mud (Fig. 4). The base of the bed has a sharp contact just above ~ 1 cm of light colored hemipelagic clay. The X-ray image shows some parallel lamination for the deepest pulse, convolute lamination (ripples) for the middle pulse, and parallel lamination for the upper pulse. The three pulses are shown by the pronounced magnetic and density peaks in the log signatures that coincide with the lighter image in the X-ray radiograph. The thick turbidite mud interval above does not exhibit structures and is homogeneous (Fig. 4; Table 1A).

Eight grain size samples have been processed (Figs. 4, 5). Below the T3 the hemipelagic clay at 110 cm, the grain size distribution curve displays a broad normal mode in very fine silt and Table 1A shows very low sand (6%) content and high clay content (29%) (Fig. 5). In the base of this turbidite T3 at 108.5 cm, the curve is bi-modal, representing two predominant grain sizes of sand and silt in the same sample (Fig. 5). This bi-modal curve coincides with the magnetic and density peaks and also with a parallel lamination of the sediment. There is the highest percent of sand (43%) and lowest % of clay (8%) in this sample (Table 1B).

Samples at 106.5 cm and 105 cm exhibit a narrower mode in the phi values of silt and sand with lower sand contents of 26% and 38 % respectively. At ~ 105 cm, the sample location coincides with the magnetic and density peaks. Also, the curve at 105 cm displays a subtle bi-modal shape. These two samples have been taken in the convolute lamination sediment interval. At 102 cm, there is a broad normal mode similar to that of the 110 cm sample, but this sample has coarser silt values ($d_{50} = 5.6 \phi$) and less clay content (15%). At 100 cm, the curve is clearly bi-modal with a high silt content (66%) that matches the third pulse peak of the log signatures and the upper parallel lamination of the sediment. At 97.5 cm the curve shows a mode in the silt values and a subtle bimodal shape hinting that there is a subtle parallel lamination of silt and sand. At 93 cm in the homogeneous dark mud at the top of the layer, the mode of the curve is narrow with fine silt phi values. Summarizing, each “apparent turbidite

pulse” is separated by a thin mud turbidite interval, but over all the multiple turbidite pulses are fining upward (Fig. 4; Tables 1A, 1B).

5.1.3. Turbidite in Willapa Canyon

Although the Willapa turbidite at 60 cm does not have a secure correlation with T3 elsewhere, sedimentologic observations and the grain size analysis of samples in 14PC have been done to do a sedimentologic characterization of proximal turbidites at the base of the slope in the northern Cascadia Basin (Fig. 4). At 60 cm there is a sandy/silty layer with a thickness of 11 cm, a muddy interval of 7 cm above and hemipelagic clay sediment below 46 cm that is inferred from visual observations and physical properties (Table 1A). The density signature shows two peaks while the magnetic log shows two weaker peaks coinciding with this turbidite bed. The base of the turbidite is sharp and scoured. Compared with the turbidites at the other Juan de Fuca at Cascadia sites, this turbidite is the coarsest ($d_{50}(\phi) = 3.6$ and 3.7) (Fig. 4; Tables 1A, 1B; Appendix 1B). Core 14 PC in Willapa Channel is located at a proximal base of slope area where coarser sediment is expected in turbidites. Also, the presence of shells, foraminifera and erosive base (features that correspond with a typical Ta Bouma sequence) suggest the proximity for this turbidite (Bouma, 1962).

In later discussions incorporating Juan de Fuca, Cascadia, Willapa and California margin channel, data will show that some of the “apparent turbidite pulses” of T3 in Cascadia Channel may be separate stacked turbidites from coeval turbidity currents that are synchronously triggered in the Juan de Fuca and Willapa tributary channel sources. However, Turbidite T3 in 14 PC of Willapa Canyon is not well correlated compared to other locations for several reasons such as insufficient forams to date. Also, the core observations and log signatures did not clearly reveal contacts between hemipelagic sediment, turbidite bases and tails because in the base of slope location, hemipelagic sediment is coarser grained than on the abyssal basin floor.

5.2. Northern California Margin

Unlike Cascadia, in the northern California margin we have not followed specific correlative turbidites because the correlations have yet to be finalized. Nevertheless, we can analyze sediment pulse features of turbidite layers and compare them with those of the Cascadia margin turbidites. We have selected representative turbidite layers from tributary channel systems and below their confluences. Detailed grain-size analyses have been completed for key layers with visually recognizable single or multiple coarse grained pulses. One goal has been to verify that pulses found in the magnetic and density logs correlate with coarse grain size. Another goal has been to outline the origin and differences between multiple pulses of an individual turbidite and stacked turbidites that deposit below tributary canyon and channel confluences. This last goal will not be fully explained until the discussion section. To simplify terminology, the coarser textural parts of turbidite units are called pulses although later in the discussion we interpret these apparent pulses to be stacked turbidites (see section 6.2).

5.2.1. Noyo Channel turbidite in 49 PC

We have described turbidite T15 that has an age of ~ 3000 Cal. yr B.P (Figs. 2, 6) (Goldfinger et al., 2007). Visually, the turbidite is made up of a 5 cm thick basal part (from 314 cm to 309 cm) of very fine sand with some mud intercalations that are capped by a 12 cm thick muddy tail (Table 2.A). No sedimentary structures are evident. There is a 6 cm layer of hemipelagic clay just below the base of this turbidite. The density log signature shows the progressive pattern of decreasing density from the base of the turbidite through the mud turbidite (tail) (Fig. 6). The magnetic susceptibility curve shows some possible subtle pulses, but the density shows that there is no other significant pulse. Consequently we interpret T15 to be a uni-pulsed turbidite in a tributary channel. At 314 cm and 312 cm, the grain size diagrams show a sandy mode whereas at 309 cm the mode is siltier (Fig. 6; Tables 2A, 2B; Appendix 2A). D50 displays a gradual gradation up the turbidite from very fine sand to coarse silt and then medium silt, which coincides with the density log signature (Fig. 6; Table 2B).

5.2.2. Gualala Channel mouth turbidite in 13PC

Site 13PC is located in the mouth of a single tributary canyon very close to multiple tributaries that join into the main proximal Gualala Channel (Fig. 2) (Goldfinger et al., 2007). Two fining up turbidite layers, a shallower uni-pulsed sand layer at 148 cm, and a more complex deeper layer at 152-156 cm have been studied (Fig. 6). The deeper layer is composed of a 6 cm graded coarse silt base deposited over a fine silt hemipelagic clay. Although the magnetic signature shows two pulses, there is a single density peak and a continuous grading of the grain size that shows it is a uni-pulsed turbidite (Fig. 6; Table 2A, 2B). Above the deeper turbidite from 152 cm to 150 cm, there is fine silt hemipelagic sediment with microfauna of foraminifera and radiolaria in the coarse fraction that separates the deeper from the shallower uni-pulsed turbidite.

Visual observation from the core lithology shows that the uni-pulsed shallower turbidite consists of a silt base from 150 cm to 148 cm, and from 148 cm to 142 cm there is a homogeneous, bioturbated turbidite mud cap with fecal pellets. At 144 cm there is a high content of silt (53%) and sand (28%), but the visual observations suggest fecal pellets instead of sand mineral grains. The magnetic log signatures and grain size bi-modal distribution display a typical mud pattern without peaks and troughs, which supports the visual observation of fecal pellets instead of sand grains.

In both set of turbidites, sandy silt bases are laminated as is observed in the core and the X-ray image, and the coarse grain size correlates with the density log peaks, lighter intensity X-ray image, and visual observations (Fig. 6; Tables 2A, 2B; Appendix 2B).

At 157.5 cm, below the base of the deeper layer, the grain size curve is broad, the percent of silt and clay are high (61% and 31% respectively) and the median is fine silt grain size (Table 2B; Appendix 2). At 156 cm and 152 cm the grain size distribution shows a sand content of 42% and 37% respectively with slightly more silt and clay content at 152 cm (46%+17%) compared to 156 cm (45%+13%) (Table 2B). At 150 cm the broad mode of very fine silt

indicates a hemipelagic mud bed similar to the sediment represented by the 157.5 cm sample (Fig. 6; Table 2B; Appendix 2B).

5.2.3. Gualala Channel turbidites in 12 PC

Three complex turbidite layers (multi-pulsed individual or stacked turbidites) are characterized in core 12PC at a channel location that is downstream from 13PC below tributary canyon confluences (Figs. 2, 6; Tables 2A, 2B).

- Deep layer (base at 225 cm):

The deepest layer analyzed in Gualala channel has a sharp erosional base at 225 cm. The layer consists of four progressively finer sand/silt pulses between 225 cm and 212 cm, with some disruption by burrows (13 cm of thickness) and capped with 3-4 cm of muddy sediment (Fig. 6, Table 2A). Gradually, a mottled burrowed mud continues in the upper part of the layer from 212 cm to 208 cm depth. The sediment is laminated as shown by the X-ray radiograph (Fig. 6). The coarsest sediment and the thickest lamina are at the base of the layers. This is shown by the core observations, a big peak in the magnetic and density signatures and a thicker lighter interval in the X-ray radiograph. Physical properties reveal a fining up sequence of pulses in the magnetic and density signatures. Grain size distribution curves show that the turbidite pulses (or individual turbidites) progressively decrease in sand content (from 57% to 25 %) and grain size (from very fine sand to medium silt), but increase in silt and clay content (> 50% of silt and 17% of clay) (Fig. 6; Tables 2A, 2B; Appendix 3).

- Middle layer (base at 203 cm):

Visually, this turbidite has a sharp planar base at 203 cm and contains several distinct very fine sand pulses that end at ~ 185 cm depth; minor sand/silt lenses continue between 185 cm to 180 cm (Fig. 6). Below the turbidite base at 203 cm, there is 5 cm of hemipelagic clay, as shown by the weak physical properties log signatures and darker colored sediment in the X-ray radiograph. Looking at the core and X-ray radiograph, sands up to 185 cm appear laminated and locally exhibit cross-bedding structures. From 185 cm to 180 cm the internal structure is

poorly developed. Physical properties display 4 sandy pulses that are difficult to distinguish visually in the X-ray radiograph (Fig. 6). Above 180 cm, the turbidite tail is represented by a mottled mud interval of 40 cm and also shown by the darker X-ray radiograph and reduced values in physical properties (Fig. 6, Table 2A).

Grain size curves at 203 cm and 199 cm are very similar and show a sand content greater than 50% at both depths (Fig. 6; Table 2B; Appendix 3). For both samples, d₅₀ is very fine sand (3.8 and 3.9 ϕ) and d₉₀ is fine sand (3 ϕ), which shows that the coarsest grain size and the median size are similar. Grain size at 202 cm and 197 cm samples are alike and exhibit a silt and sand bi-modal shape, high clay content and representative d₅₀ in the medium and coarse silt grain sizes respectively. In summary, grain size at 203 cm and 199 cm represent the first two coarse-grained sediment pulses that coincide with the two peaks of the magnetic logs (Fig. 6; Table 2B; Appendix 3). The silty mud between pulses is shown at 202 cm and 197 cm. A third coarse-grained pulse begins at ~ 192 cm and continues until ~ 187 cm. The fourth pulse is located at about 185cm and coincides with a pronounced but thin peak of the magnetic log signature. Summarizing, the middle turbidite layer with base at 203 is ~ 23 cm thick and contains three coarsening up pulses at the bottom and a minor fining up pulse at the top.

- Shallow layer (base at 58 cm):

The shallow turbidite layer has a sharp flat base at 58 cm, but has a gradational upper boundary. The layer is composed of progressively finer bioturbated sandy bi /tri-pulses or lenses from 58 cm to 50 cm as shown by the density and magnetic log signatures and the X-ray radiograph. The sandy turbidite base is overlain by a muddy mottled interval that continues to the core top. Hemipelagic sediment underlies the turbidite because a coarse fraction sample at 62 cm has a high content of radiolaria and scarce terrigenous material (Table 2A).

At 58 cm there is the highest content of clay (22%) compared with the other samples (Table 2B; Appendix 3). This basal turbidite sand appears to have some underlying hemipelagic sediment mixed into it by bioturbation which explains the anomalous shape of the grain size histogram and the high clay and sand contents simultaneously. At 56 cm and 53 cm the mode is sandy for both samples; however, the content of sand is higher and the content of clay is lower

at 53 cm and coincides with the highest peak of the physical properties. The clay content progressively decreases toward the upper part of the sandy and silty pulses at 56 cm and 53 cm. There is an apparent lack of correspondence between the physical properties and the grain size trends, shown by a progressive decrease in the magnetic and density values, which suggests a fining up sequence and contradicts the grain size pattern. This fact can be explained because of the lenticular character of the beds, making the bed not continue laterally and hence, altering the signature of the physical properties.

5.2.4. Noyo/Gualala/Viscaino confluence turbidites in 24GC

Two turbidite layers with bases at 42 cm and 57.5 cm respectively and separated by ~ 3 cm of hemipelagic clay sediment have been characterized independently, however, their interpretation has been treated jointly (Figs. 6, 7; Tables 2A, 2B; Appendix 4).

- Deep layer (base at 57.5 cm):

The deep layer has the base at 57.5 cm and it is composed of two coarse-grained pulses with 2 cm and 3.5 cm thickness respectively. These pulses are separated by a 2.5 cm siltier interval, shown by the darker colour in the X-rays and lower value of the magnetic log. The base of the lower pulse is sharp, and the base of the upper pulse is irregular. The upper pulse grades into an 8.5 cm mud turbidite tail. Below the coarse-grained pulses, there is 4.5 cm of hemipelagic clay. The clay is well shown by the dark color of X-radiograph and low values of magnetic susceptibility logs, as well as the visual observations of the core.

At 59 cm in the hemipelagic mud, below the lower pulse and turbidite base, the broad shape of the grain size mode is dominated by silt and clay (more than 90%). At 57 cm and 54 cm the grain size samples were taken from the sandy/ silty pulses. More than 90 % sand is found in both samples but more than one grain size is represented by the d50 and d90 at 54 cm (5.7 and 1.2 ϕ respectively). However, similar modes of d50 and d90 suggest just one representative grain size of medium sand at 57 cm. There is a good correspondence between the grain size of pulses and the high peaks of the magnetic and density signatures. A siltier interval at 55 cm has

heterogeneous grain size as is shown by the broad mode and irregular grain size curve; a silt matrix predominates compared with the rest of the sizes. The mud tail at 52 cm contains a high sand content (35%) (Tables 2A, 2B; Appendix 4).

As stated in the Previous Results section, mineralogic analysis has been done for this turbidite at 53 and 56 cm (Fig. 3B). Tributary canyons have specific mineral content and feed downstream turbidite channels. These mineral assemblages of the tributary canyon sources can be correlated with the coarse grained pulses that form the turbidites. The homogeneous medium sand pulse at 57 cm contains Viscaino Channel sand and, the heterogeneous grain size sand pulse at 54 cm contains Gualala mixed minerals (Figs. 3B, 6) (Goldfinger et al., 2007).

- Shallower layer (base at 42cm):

Visually, the upper layer with a base at 42 cm is composed of three sandy and silty fining upward coarser-grained pulses that have sharp bottoms with each pulse gradually becoming thicker from the base to the top of the turbidite (~1-3 cm thick). Each sequence is truncated by the overlying pulse. The last pulse has a gradational top above 35 cm. Pulses are separated by 0.5 cm to 1 cm of muddy sediment, but there is no hemipelagic sediment between the sandier pulses. From 35 cm to 13 cm there is a bioturbated turbidite mud interval. The sandy pulses are also shown also by the three peaks of the magnetic log signature and the light intervals of the X-radiograph. Internal sedimentary structures are not observed in the pulses (Figs. 6, 7; Tables 2A, 2B).

The grain size analysis at 41 cm, 39 cm and 35.5 cm correspond with the sandy/silty pulses. At 41 cm and 35.5 cm the grain size distribution is clearly bi-modal in the silt to sand sizes with more than the 50% and 79 % sand respectively (Fig. 7; Table 2B). However, at 39 cm the grain size curve has a narrow mode with almost 100% medium sand content as shown in the table 2B. There is good correspondence of the coarser grain size with the peaks of the magnetic signatures. Samples taken at 40 cm and 37.5 cm correspond with the inter-pulse muddier interval. At 40 cm the grain size curve is very broad and represents a heterogeneous grain size distribution ($d_{50} = 5.9 \phi$ and $d_{90} = 1.8 \phi$), but there is a predominance of mud (~ 70%) (Table 2B). At 37.5 cm the grain size is bi-modal with sand and silt grain sizes, but contains a majority

of silt and clay (67%). At 34 cm the grain size curve is a typical muddy interval containing a little sand and corresponding to the turbidite tail. At 42 cm, below the base of the lower pulse, the grain size curve shows typical muddy hemipelagic sediment composed of more than the 90 % silt and clay.

Mineralogical analyses have been done for the sandy and silty pulses at 35, 36 and 39 cm (Figs. 3B, 6) (Goldfinger et al., 2007). For the lower pulse at 41 cm, the bi-modal grain size curve is associated with the mineral provenance of the Arena/Gualala canyons. The ~ 100% medium sand pulse at 39 cm corresponds with the provenance of the Viscaino Channel. The upper pulse at 35 cm contains the Gualala mixed mineral provenance.

5.2.5. Gualala/Viscaino /Cordell confluence turbidites at 31PC

There are two closely spaced layers selected from this site. The layers start at 85 cm of depth and extend until the core top. There is a deeper bi-pulsed layer of sand/silt from 85 cm to 65 cm, a muddy interval from 65 cm to 60 cm and a tri-pulsed layer of sand/silt from 60 cm to 32 cm. Above 32 cm, there is a bioturbated turbidite mud tail. The coarse-grained pulses are laminated and the bases are sharp (Fig. 6; Tables 2A, 2B; Appendix 5).

At 87 cm in the hemipelagic sediment below the turbidite layer, the wide mode of the grain size curve shows predominantly very fine silt ($d_{50} = 7.2 \phi$). At 83.5 cm, the grain size distribution has a mode of fine to medium sand, and the turbidite is almost 100 % sand (Table 2B). This sample coincides with the first pulse at the base of the deeper turbidite. At 73.5 cm and 66 cm, the grain size distributions of the upper pulse of the deeper turbidite are very equal with modes of coarse silt ($d_{50} = 4.1$ and 4.4ϕ respectively). At 56 cm, the lower pulse of the shallow layer has a coarse silt mode (85%) (Table 2B; Appendix 5). At 52.5 cm, the lower part of the second pulse of the layer exhibits a narrow mode with d_{50} of coarse silt (Table 2A; Appendix 5). The second pulse is also represented by a sample at 48 cm where the silt content is predominant (87%) with d_{50} of medium silt (Appendix 5, Table 2A). The third pulse of the layer is represented by the samples at 38.5 cm and 34.5 cm that are dominantly silt (> 50%)

with more than 20% sand (Table 2B). The turbidite mud tail at 31 cm has higher silt /clay, lower sand content and the curve mode has a broad shape.

Mineralogic analysis has been done on the coarse-grained pulses of 31PC. At 84 cm there is a bi-modal population of coarser grains with a Viscaino source (no heavy minerals), whereas the fine-grained fraction contains heavy/mafic minerals indicative of the Gualala source (Goldfinger et al., 2007). This mineralogical sample coincides with the higher sand content and larger grain size at 84 cm. This pattern is similar to that shown in an analogous turbidite of the 24CG core (Figs. 3B, 6). At 75 and 71 cm, mineral samples show a Gualala provenance rich in heavy minerals that coincides with the base of the upper pulse of the deeper turbidite in 31PC. The same trend is also exhibited in the deeper bi-pulsed turbidite of the 24GC core (Figs. 3B, 6).

6. DISCUSSION

6.1. Features of turbidites in Cascadia Margin

The sedimentologic features of Holocene turbidites as well as the physical properties and radiocarbon ages from the active tectonic continental margin of Cascadia can be utilized to document their seismic origin and correlation of individual turbidites at different locations throughout Cascadia Basin (Nelson et al., 2000; Goldfinger et al., 2003a, 2003b, 2008, 2012, Gutierrez-Pastor et al., 2009). Thus, we can compare the sedimentologic variations of the same turbidite from proximal to distal locations in channels such as turbidite T3 from the more proximal Juan de Fuca Channel and the distal Cascadia Channel site below the confluence of the proximal channel tributaries (Figs. 1, 4; Tables 1A, 1B).

The first important result is that, the grain size analyses of turbidites along the Cascadia margin verify physical properties peaks as proxies for coarser-grained turbidite pulses and that density is the most reliable proxy for sediment texture. For example, all density log pulses shown in figures 3, 4 and 6 (e.g. T3 of 25PC in Cascadia Channel, T15 of 49PC in Noyo Channel, turbidites of 12PC and 13 PC in Gualala Channel) show a clear correspondence

between grain size and density log signatures. Generally, magnetic susceptibility log signature pulses also correlate with grain size with a few exceptions (e.g. T3 in PC12 of Juan de Fuca Channel and PC 13 of Gualala Channel) (Figs. 4, 6).

The textural data supports Goldfinger et al. (2008, 2012) physical properties studies that use the number and character of turbidite pulses as criteria to correlate turbidites from different channels (Fig. 3C). In addition, Goldfinger et al. (2012 see Fig. 47A) shows that there are nearly perfect Pearson correlation coefficients (0.84 to 0.95) for pulses per event in 18 correlative turbidites from 4 different types of turbidite systems for 600 km along the Cascadia margin. These data show that the physical property pulse signatures of correlated turbidites is the same upstream and downstream of channel confluences in the same turbidite system and throughout channels of all different Cascadia turbidite systems (Fig. 8). Figure 8 summarizes the number of turbidite pulses for the 18 correlative turbidites of Juan de Fuca and Cascadia Channels. The histogram of pulses per turbidite compiled in this study and previous work shows that, during the Holocene along ~ 600 kilometers of the Cascadia Basin, there is a predominance of multi-pulsed seismo-turbidites both upstream and downstream below channel confluences (Fig. 8) (Goldfinger et al., 2008, 2012).

The historical 1700 A.D. earthquake event in the Cascadia subduction zone (e.g. Nelson et al., 1995; Satake et al. 1996, 2003) corroborates that multi-pulsed turbidites characterize Cascadia Basin, and suggests that the correlative pulses may be related to the original seismic shaking signature of each individual great earthquake. Goldfinger et al. (2012 see Fig. 47A) show that the T1 turbidite, correlated with the A.D. 1700 earthquake, has 2 pulses in four widespread locations in different turbidite systems (Fig. 8). Previously, we have postulated that earthquake shaking signatures apparently create the turbidite pulses, because this 1700 A.D. historical turbidite and most other correlative Holocene turbidites from widespread different turbidite systems (e.g. Juan de Fuca Channel, Cascadia Channel, Hydrate Ridge intraslope basin, and Rogue Apron) have the same multi-pulsed grain-size signatures shown by physical property logs (Fig. 8) (Goldfinger et al., 2008, 2012 see Fig. 47A).

Further evidence for this hypothesis is that, similar to pulse signatures, the thickness of each correlative T1 to T18 seismo-turbidite is consistently the same throughout Cascadia Basin (Figs. 3C, 8). Goldfinger et al. (2012 see Fig. 47B) again shows that there is an excellent Pearson correlation coefficient (generally 0.7 to 0.96) for thickness per event in 18 correlative turbidites from 4 different types of turbidite systems for 600 km along the Cascadia margin. Given the heterogeneity of turbidity current processes and deposition, it is remarkable that these correlative turbidite pulse and thickness patterns are so consistent throughout northern Cascadia Basin. As we have postulated earlier (Goldfinger et al., 2008, 2012), and further confirmed with sedimentologic characteristics in this paper, earthquake shaking seems to be the most plausible explanation for these synchronous correlative turbidite pulses and thicknesses in Cascadia Basin during the Holocene.

Although multi-pulsed turbidites are dominant, uni-pulsed turbidites, occasionally are found in Cascadia Basin (e.g. 11% in Fig. 8). For example, turbidite T3 in Juan de Fuca Channel (12PC) has a density signature with one uni-pulsed (single fining up) peak compared to the two peaks of the magnetic signature (Fig. 4). The grain size, however, shows a single fining up graded layer that is a uni-pulsed turbidite. The density log is clearly bi-pulsed for T3 in 12TC, the trigger core for 12PC, although T3 in 11TC (the same location as 12 PC) shows the same physical property signatures as those in 12PC (one peak in the density log and two peaks in the magnetic log) (Goldfinger et al., 2012 see Fig. 19). In summary, T3 at the same Juan de Fuca Channel location shows evidence for both uni and multi-pulsed characteristics. However, the clear bi-pulsed density log in 12TC and other locations (Goldfinger et al., 2012), and the consistent bi-pulsed magnetic logs that may detect a subtle pulse not detected by density, indicate that this is a bi-pulsed turbidite. Downstream in Cascadia Channel below the Juan de Fuca and Willapa Channel confluences, T3 clearly has 3 pulses and is thicker and coarser grained than T3 in the Juan de Fuca tributary channel.

We believe that the variable sedimentologic characteristics and physical property log signatures of the Juan de Fuca T3 turbidite result from variable deposition and erosion in the proximal channel setting of the 11TC and 12PC/TC cores (Figs. 1, 4). Our swath bathymetric studies

have shown a complex morphology in many proximal channels of Cascadia Basin (e.g. Juan de Fuca, Astoria, Trinidad, Eel) (Nelson et al., 2000). In other high-resolution deep-tow sidescan images of the Var and Laurentian proximal fan channels, a complex physiography of scours, bedforms and non-deposition is observed (Malinverno et al., 1988; Piper et al., 1999). From these observations, we surmise that it is most likely that the second pulse in some locations is missing from erosion or non-deposition, rather than that a second coarse-grained pulse has been added at some core sites and not at others. We also apply the same non-deposition/erosional explanation for the T14 and T15 turbidites that exhibit half uni-pulsed and half bi-pulsed log signatures at different Cascadia Basin locations (Goldfinger et al., 2012 see Fig. 47). This leaves only T2, and T12 turbidites, or 11%, that are uni-pulsed both upstream and downstream in Cascadia Basin channels. For these rare uni-pulsed turbidites, given the heterogeneity of earthquakes in any fault system, we postulate that occasionally weaker Cascadia earthquakes do not trigger multi-pulsed turbidity currents and only deposit uni-pulsed turbidites throughout the proximal and distal parts of turbidite systems (Fig. 8). A further explanation for this hypothesis is provided in more detail in section 6.3 of this discussion.

The T3 bi-pulsed turbidite of proximal Juan de Fuca is correlative with the tri-pulsed T3 turbidite layer in Cascadia Channel downstream from the confluence of Juan de Fuca and Willapa channels (Figs. 1, 8) (Goldfinger et al., 2008). The T3 sediment in Cascadia Channel is derived from different tributary channels with separate turbidity currents that have been synchronously triggered by the same great earthquake. The separate turbidity currents arrive at the downstream Cascadia Channel site at different times, depending on the sediment volumes and distance from the source to the deposition site. The arrival of these currents within a short time span explains the lack of hemipelagic sediment between different turbidite pulses and/or possible stacked turbidites from multiple tributary sources (Fig. 3).

Also, the multiple additive sediment sources from different tributary channels most likely explain why the T3 turbidite in Cascadia Channel is thicker than T3 in the more proximal Juan de Fuca and Willapa sites. The upstream tributary sources also suggest an answer for why the T3 turbidite in Cascadia Channel is coarser grained compared with T3 found upstream in Juan

de Fuca Channel (Fig. 4; Table 1B). The sediment of Willapa Canyon and Channel is coarser grained compared to Juan de Fuca Channel (Fig. 4). Willapa Channel is the southernmost and closest tributary to Cascadia Channel (Fig. 1). The coarsest Columbia River sediment is deposited on the Washington shelf closest to the Willapa Canyon head compared to the finer shelf sediment that is deposited near the more distal Juan de Fuca Canyon head (Fig. 1) (Sternberg, 1986; Wolf and Hammer, 1999). For this reason, we hypothesize that the coarse sediment from Willapa Channel results in a coarser grained T3 turbidite in Cascadia Channel compared to T3 in Juan de Fuca Channel (Fig. 4; Table 1B).

In summary, the visual core descriptions, grain-size analyses, physical properties log signatures and their geographic distribution indicate that the dominantly multi-pulsed seismo-turbidites in Cascadia Basin result from original great earthquake shaking and aftershocks (Fig. 8); however occasional weaker earthquakes result in uni-pulsed turbidites upstream and downstream. In some cases, such as in Cascadia Channel T3 below tributary confluences, a turbidite may be both multi-pulsed and stacked.

6.2. Features of turbidites in the Northern California Margin

The northern California margin turbidites also are interpreted to be triggered by earthquakes based mainly on correlations of physical properties and radiocarbon ages. Goldfinger et al. (2007, 2008) affirm that the physical properties are the fingerprints of each turbidite and thus the same turbidite can be correlated in different channel systems separated by hundreds of kilometers along the margin. There are characteristic lithologic, physical property log signatures and grain size patterns of the seismo-turbidites that are related to northern San Andreas Fault earthquakes (Figs. 2, 3, 6).

We find that there is a dominance of uni-pulsed turbidites in single tributary canyon and channels such as Noyo Channel and Gualala Canyon (Figs. 2, 6). In Noyo Channel ten of the first eleven turbidites are uni-pulsed (Fig. 9). New CT scan data for all 39 turbidite events in Noyo 49 PC shows only four certain multi-pulsed turbidites (10%) and two more equivocal

multi-pulsed turbidites (5%) or a range of 10-15% multi-pulsed turbidites (Goldfinger et al., unpublished data). Several other cores in Noyo Channel contain 12-19 % multi-pulsed turbidites (Goldfinger et al., 2007, 2008). Looking at the entire 13PC core in the single Gualala tributary canyon, we find that nine turbidites are uni-pulsed and two uni-pulsed turbidites may have weak multiple coarse units (Goldfinger et al., 2007). This dominance of uni-pulsed turbidites in Noyo proximal channel and Gualala tributary canyon suggests that the generally weaker earthquakes of northern California margin (≤ 8 Mw) result in dominantly uni-pulsed turbidites in proximal tributary canyons and channels with simple morphology (i.e. without other tributaries) and that the strongest earthquakes may be responsible for the few multi-pulsed turbidites in tributary canyons and channels (Figs. 3C, 9).

Further confirmation of the dominance of upstream uni-pulsed seismo.-turbidites is provided by the historical 1906 Mw 7.9 earthquake that affected the entire northern California margin from Monterey Bay to the Mendocino Triple Junction (Fig. 2). The T1 uni-pulsed turbidite related to this San Andreas 1906 earthquake is well dated at several locations by ^{14}C and the thickness of hemipelagic sediment overlying it (e.g. sediment thickness/sedimentation rate = age) (Fig. 9) (Nelson et al., 2000; Goldfinger et al., 2007). The T1 turbidites of Box 1 and PC 51 in Mendocino Channel, 49PC in Noyo Channel, and 13 PC in the Gualala Canyon mouth all exhibit uni-pulsed physical property log signatures (Fig. 9) (Nelson et al., 2000; Goldfinger et al., 2007, 2008).

In contrast with the 13PC uni-pulsed turbidites in the Gualala tributary canyon, the 12PC turbidite layers 20 km downstream in the main Gualala Channel, and located below multiple Gualala tributary canyons have several units with sediment that fine-upward or coarsen upward (Figs. 2, 6; Table 2A). Also examination of the physical properties and lithology throughout core 12PC shows that 12 turbidites have multiple coarse units and 2 possibly are uni-pulsed (Goldfinger et al., 2007). The characteristics of the turbidites at 12PC relate to the close proximity of the multiple canyon tributaries and the different times of turbidity-current arrival at the site (Fig. 2). At 12 PC below the confluence of multiple tributary canyons, as expected, we find thicker turbidites than in the 13 PC tributary canyon (Fig. 6). An example, of this

thickening below a confluence is shown by the upstream turbidite layer with a base at 157 cm in 13PC that Goldfinger et al. (2007) have correlated based on physical properties to the thicker turbidite with a base at 203 cm in 12PC (Fig. 6).

Although the gradual seafloor erosion and incorporation of particles within a single turbidity-current event can also explain the increasing thickness of turbidites along a canyon/channel, in this case the thicker bed is related to its location below many tributary canyon sources that provide nearly synchronous multiple inputs of sediment (Figs. 2). The different mineralogy of these coarse-grained sub-units proves that these sediment inputs are additive to create the thicker turbidite below the tributary canyon confluences (Fig. 3B).

Downstream from the confluences between Noyo, Gualala, Viscaino and Cordell channels, the grain-size analyses of turbidites at 24GC and 31PC, again correlate with physical property logs that exhibit multiple coarse-grained units in the turbidite event (Figs. 2, 3B, 6). The lack of hemipelagic sediment intervals between these multiple coarse grained units indicates that they deposited during a short interval of time (Figs. 3B and 6). Only the last coarse-grained sub-unit has a tail, indicating final waning of a turbidity current. We interpret that these multiple coarse units are triggered by a single earthquake event because synchronous triggering in multiple tributary canyons results in the arrival of several nearly synchronous turbidity currents below the confluence of tributary canyons and channels. This is proven by the facts that 1) each coarse unit has a distinct mineralogy from different tributary canyons and channels and 2) there is no hemipelagic sediment between units.

Originally, these coarse units have been attributed to be part of a multi-pulsed individual turbidite; however, the dominance of uni-pulsed Noyo Channel and Gualala canyon turbidites from a canyon with no tributaries and dominance of multiple coarse units from downstream channels with several canyon tributaries, and most important, the different mineralogical evidence for each of the coarse units, lead us to interpret that these apparent multi-pulsed turbidites in 12PC, 24GC, and 31PC below confluences are stacked turbidites deposited from synchronously triggered turbidity currents in multiple tributary canyons (Figs. 3B, 6). Similar turbidite characteristics have been observed in Lake Zurich, Switzerland, where multiple

landslides along the lake basin walls are synchronously triggered by an earthquake and then the multiple coeval turbidity currents derived from the landslides deposit stacked turbidites on the lake basin floor (Strasser et al., 2006).

Below the Gualala/Viscaino confluence, we observe that the deeper Viscaino stacked turbidite arrives first. The Viscaino sands are coarser and more mature (without mafic minerals) that have been weathered, eroded, and transported by littoral drift northward along the coastline (Fig. 3B). The Viscaino canyon head intersects the littoral drift along the shoreline and collects the coarser sand that later feeds the turbidites (Fig. 2). Viscaino turbidity currents with coarser sand, and possibly greater volume because of the active littoral drift source, apparently have a greater velocity and they arrive first to deposit the lower/middle pulses of turbidites below the Noyo/Gualala/Viscaino confluence, even though the Gualala sands travel a shorter distance to this site (Figs. 3B, 6; Table 2B). Also note that there is apparent reverse grading in the stacked turbidites of 24GC. Reversely graded beds in 24GC could result from the erosion of the previous bed by the turbidity current from a tributary and incorporation of the sediment in the bed deposited immediately above. However, the lack of truncation in the underlying turbidite top in 24GC, and presence of reverse grading also in 12PC and 31PC suggest that reverse grading is a feature of some stacked turbidites.

The provenance input of 31PC is less distinct than 24GC, suggesting further mixing of mineralogy downstream (Fig. 3B). Site 31PC, which is actually below a total of four confluences, has an input from a total of six channels, while site 24GC has input from only three channels (Fig. 2) (Goldfinger et al., 2008). We infer that synchronous triggering in multiple canyon heads is the best explanation for the stacked turbidites that are observed below confluences along the northern California margin. Non-synchronous triggering should produce an additive turbidite record that increases in complexity below each confluence. The mixing and stacking of the mineral provenance components confirms the nearly synchronous arrival of stacked turbidites below the channel confluences. A similar use of mineralogic provenance to fingerprint source channels and test for earthquake origin has been used in the Sea of Japan by Shiki et al. (2000). Our results help substantiate the earthquake origin for turbidites that has

been postulated by Goldfinger et al, (2007, 2008) for the northern California margin associated with the San Andreas Fault (Fig. 2).

6.3. Comparison between features of turbidites at Cascadia and northern California margins and implications for other active and passive margins

Even though Cascadia and northern California margins have different tectonic settings, both active margins contain comparable turbidites, because they are triggered by great earthquakes (Fig. 10). In single tributary canyons or proximal channels without multiple tributary canyons (e.g. Juan de Fuca, Noyo, Gualala canyon) uni-pulsed turbidites are observed. At these proximal sites, the uni-pulsed turbidites exhibit a single fining upward sequence and do not contain well-developed internal sedimentary structures or show subtle lamination (Figs. 4, 6, 10; Tables 1A, 2A). Although proximal uni-pulsed turbidites are, dominant in Noyo Channel and Gualala canyon, and a few are found in Cascadia channels, nearly all turbidites are multi-pulsed or stacked below canyon and channel confluences in Cascadia and California margins (Figs. 1, 2, 3, 6, 10) (Goldfinger et al., 2003a, 2003b, 2007, 2008).

Rare turbidites of (e.g. T2, and T12) of Cascadia Basin channels are uni-pulsed both upstream and downstream (Figs. 4, 8) (Goldfinger et al., 2012). In another rare case, T3 in Juan de Fuca Channel correlates downstream below the confluence with Cascadia Channel T3 that has 3 coarse-grained units (Figs. 4, 8). These data suggest that occasionally there is some stacking and mixing from synchronous earthquake triggering in multiple canyon sources and deposition from coeval turbidity currents (Tables 1A, 1B). As outlined previously, because most upstream and downstream correlative turbidites exhibit the same multi-pulsed characteristics, (Goldfinger et al., 2012), we interpret that these coarse-grained pulses are generated by the original earthquake and/or aftershock rupture patterns of the strongest earthquakes (~ 9 Mw) (Fig. 3C). Generally in Cascadia Basin, the uni-pulsed turbidites (e.g. T2, T12) are also the thinnest turbidites, which suggests that turbidites from occasional weaker

earthquakes ($\sim <9$ Mw) may not develop multiple pulses (Fig.8) (Goldfinger et al., 2003, 2012 see T2 and T12 in Fig. 47B).

In contrast to the dominance of multi-pulsed turbidites in tributary canyons and channels of Cascadia, uni-pulsed turbidites dominate in tributary canyons and channels of the San Andreas California margin (Figs. 6, 8, 9). Because 1) upstream California tributaries have mainly uni-pulsed turbidites, 2) most of the turbidite event layers with multiple coarse-grained units are found downstream in channels below the confluences of multiple tributary sources, and 3) each coarse unit has specific mineralogy of a tributary canyon source, we interpret that downstream California turbidite layers with multiple coarse units are stacked turbidites compared to the dominant upstream and downstream multi-pulsed individual turbidites in Cascadia.

We postulate that California turbidites are mainly uni-pulsed at proximal locations above confluences because of shorter fault rupture lengths and historical weaker earthquakes (~ 200 km ruptures and ≤ 8 Mw) (Goldfinger et al., 2008) along the northern San Andreas California margin compared to the longer rupture lengths and stronger earthquakes (~ 600 to 1000 km ruptures and ~ 9 Mw) (Satake et al., 2003; Goldfinger et al., 2012) of the Cascadia subduction margin whose earthquake shaking apparently creates multi-pulsed proximal turbidites. Stacked turbidites characterize the San Andreas margin below tributary confluences, because of the morphology of the margin that has multiple tributary sources and channel confluences where synchronously triggered turbidity currents deposit (Figs. 2, 10). In contrast, multi-pulsed turbidites are characteristic upstream and downstream throughout Cascadia margin channels because of the primary shaking signatures of the strong Cascadia margin earthquakes (Figs. 3C, 6, 8, 10).

Nakajima and Kanai (2000) as well as Shiki et al. (2000) studied seismo-turbidites from the Japan Sea plus Lake Biwa, and Gorsline et al., (2000) analyzed turbidites from the Santa Monica and Alfonso basins, California. Nakajima and Kanai (2000) observed that turbidites triggered by earthquakes exhibit different characteristics than those classic turbidites described by Bouma (1962) that appear to generate from non-seismic mechanisms. In active tectonic margins with strong earthquakes, Nakajima, Shiki and Gorsline found that turbidites had wide

areal extent, exhibited multi-pulsed beds, irregular sedimentary structures, grain-size breaks/fluctuations, abrupt changes in composition within the bed, variable composition among beds and greater depositional volume than turbidites triggered by other mechanisms

Our studies confirm these observations in seismo-turbidites that have detailed stratigraphic, age and physical properties correlations along entire continental margins and throughout channels. In addition, we can show proximal to distal variations in seismo-turbidites that are related to earthquake strength plus canyon and channel morphologic settings, within the same margin and between different margins. We also show that synchronous earthquake triggering in multiple canyon heads with different mineral sources results in stacked turbidites containing different mineralogies (Figs. 3, 10).

The classic literature of turbidites explains the amalgamation of turbidite beds as the result of the erosion of a later separate following turbidity current. Sequential turbidity currents may erode into the previous turbidite deposits resulting in an amalgamated turbidite with one or several beds truncated by the erosion of different turbidity currents that follow years to hundred of years later. We show that synchronous multiple turbidity currents from different tributary canyons that are triggered by an earthquake travel thorough the confluences of tributary canyons or channels and arrive at slightly different times to deposit stacked turbidites in the same downstream site. These stacked turbidites, as well as multi-pulsed turbidites create another type of amalgamated bed that is generated by a single earthquake event.

Although multi-pulsed turbidites are characteristic of the Cascadia Basin turbidite systems and some reverse grading of stacked turbidites is observed, these characteristics are not unique to seismo-turbidites. Multiple pulses with reverse grading, within an individual turbidite, have been interpreted to characterize turbidites from hyperpycnal flows (i.e. hyperpycnites) (Mulder et al., 2003). Outcrops of inner levees along thalwegs of turbidite channels and mini-basin margins also exhibit multi-pulsed turbidites (Kane and Hodgson, 2011; Kneller and McCaffrey, 2003). Consequently, multi-pulsed turbidites and reverse grading are not an unique criteria for seismo-turbidites, levee turbidites, or hyperpycnites.

In comparison to active tectonic margins, turbidites in passive muddy margins appear to be mainly generated during low stands of sea level and by non-seismic mechanisms such as storms, floods or sediment failures resulting from overloaded and under consolidated slope sediment (e.g. Nelson et al., 1992; Tripsanas et al., 2006; Twichell et al., 1992, 2000, 2009). The typical muddy and unstable slopes of deltaic margins off large rivers in passive margins result in combined turbidite and mass transport systems that may be different from those in active tectonic margins (Nelson et al., 2011).

Turbidites in passive margins appear to mainly have simple fining upward grain size rather than being mainly multi-pulsed or stacked as they are off the active tectonic margins of western North America. Along the Ebro and the Mississippi deltaic margins, simple fining upward turbidites are most common (Nelson and Maldonado, 1988; Nelson et al., 1992, 2009, 2011 Twichell et al., 2000, 2009). In Bryant Canyon mini-basins, Twichell et al. (2000) and Tripsanas et al. (2006) found classic graded sand beds and muddy turbidites in the overbank deposits with the complete mud turbidite sequence of Stow and Shanmugam (1980). Although there appear to be some general differences in sedimentologic characteristics that distinguish turbidities triggered by earthquakes compared to those triggered more commonly by other mechanisms in passive margin settings, additional studies are necessary to verify these preliminary suggestions.

7. CONCLUSIONS

1. Grain-size analysis verifies that physical properties, particularly density, are accurate proxies for coarse-grained sediment pulses in turbidites of the Cascadia Basin and stacked turbidites of the northern California active tectonic margins.

2. The grain size and physical properties show that there are three characteristic types of seismo-turbidites in both active tectonic margins: 1) uni-pulsed individual turbidites with simple fining upward grain-size gradation similar to classic turbidites; 2) multi-pulsed

individual turbidites with multiple coarse-grained pulses within the individual turbidite that are deposited from the same turbidity current; and 3) stacked separate turbidites that are deposited nearly synchronously from coeval turbidity currents that deposit downstream below tributary canyon or channel confluences. Both individual multi-pulsed and stacked turbidites have no hemipelagic sediment between pulses or stacked turbidites, which verifies their nearly synchronous deposition.

3. In general, Cascadia Basin individual seismo-turbidites triggered by the typically strong great earthquakes (~ 9 Mw) on the Cascadia Subduction Zone have correlative multi-pulsed physical property signatures throughout all canyons and channels. However, a few uni-pulsed turbidites, apparently from occasional weaker (~ 8 Mw) earthquakes are found upstream in, single tributary canyons or channels.

4. In general, northern California seismo-turbidites triggered by weaker great earthquakes (up to ~ 8 Mw) on the San Andreas Fault, are uni-pulsed in single tributary canyons and channels, and are stacked in channels below tributary confluences.

5. Along active tectonic margins, individual seismo-turbidites generated by the strongest great earthquakes (~ 9 Mw) are dominantly multi-pulsed throughout entire turbidite systems, apparently because they retain the unique shaking signature of each (~ 9 Mw) earthquake. Seismo-turbidites generated by the weaker great earthquakes (~ 8 Mw), are uni-pulsed in tributaries and become stacked turbidites in channels below tributary confluences where coeval turbidity currents deposit.

6. Origin of stacked turbidites from synchronous earthquake triggering is shown by their greater thickness compared to correlative upstream turbidites, variable grain size contributed by the different tributary sources, and specific mineralogy of each stacked turbidite that is correlative with the specific mineralogy for each tributary canyon source.

7. The generation of multi-pulsed turbidites or stacked seismo-turbidites from synchronous earthquake triggering of turbidity currents in tributary canyons along active tectonic margins provides another explanation for amalgamated turbidites.

8. The reverse grading in sediments is not unique criteria for hyperpycnites, thalweg levee turbidites, or mini-basin margin turbidites.

9. Although further research is required, multi-pulsed and stacked turbidites appear to characterize active tectonic margins, whereas preliminary evidence suggests that classic simple fining upward turbidites are more common in passive margins.

ACKNOWLEDGEMENTS

We are especially grateful to the crews of the Scripps Institute of Oceanography ships R.V. Melville and R.V. Roger Revelle and to the members of the 1999 and 2002 Scientific Parties: Mike Winkler, Pete Kalk, Antonio Camarero, Clara Morri, Gita Dunhill, Luis Ramos, Alex Raab, Nick Pias Jr., Mark Pourmanoutscheri, David Van Rooij, Lawrence Amy, Churn-Chi “Charles” Liu, Chris Moser, Devin Etheridge, Heidi Stenner, Chris Popham, Claire McKee, Duncan MacMillan, Chris Crosby, Susanne Schmid, Eulalia Gracia, Suzanne Lovelady, Chris Romsos, Jason Chaytor, Vincent Rinterknecht, Rondi Robison, David Casas, Francois Charlet, Britta Hinrichsen, Jeremiah Oxford, Miquel Marin, Marta Mas, Sergio Montes, Raquel Villalonga, Alexis Vizcaino, Santiago Jimenez, Mayte Pedrosa, Silvia Perez, Jorge Perez, Andreu Turra, David Lamas, Himar Falcon, and Andres Barranco. We thank the Active Tectonics Group at Oregon State and James H. Power from the U. S. Environmental Protection Agency at Newport, Oregon, for providing the use of the Laser Diffraction Particle Size Analyzer for grain size analysis. We gratefully acknowledge funding by the US National Science Foundation (Awards: 0107093 and 0001074) and U.S. Geological Survey for this research (Awards: GRANT00017981, GRANT00018360, 04HQGR0063, 03HQGR0008, 03HQGR0006, 02HQGR0034, 02HQGR0043) and the Ministerio de Educación y Ciencia (Award CGL2006-27096-E/BTE) and Consejo Superior de Investigaciones Científicas (CSIC)-Spain (Award: PI 2006 3 01 021).

REFERENCES

- Adams, J., 1990. Paleoseismicity of the Cascadia Subduction Zone: evidence from turbidites off the Oregon-Washington margin. *Tectonics* 9, 569-583.
- Atwater, B.F., 1987. Evidence for great Holocene earthquakes along the outer coast of Washington State. *Science* 236, 942-944.
- Atwater, B.F., Hemphill-Haley, E., 1997. Recurrence intervals for great earthquakes of the past 3500 years at northeastern Willapa Bay, Washington. U.S. Geological Survey Professional Paper, 1576, 108 pp.
- Atwater, B.F., Nelson, A.R., Clague, J., Carver, G.A., Yamaguchi, D.K., Bobrowsky, P.T., Bourgeois, J., Darienzo, M.E., Grant, W.C., Hemphill-Haley, E., Kelsey, H.M., Jacoby, G.C., Nishenko, S.P., Palmer, S.P., Peterson, C.D., Reinhart, M.A., 1995. Summary of coastal geologic evidence for past great earthquakes at the Cascadia subduction zone. *Earthquake Spectra* 11, 1-18.
- Blott, S.J., Pye, K., 2006. Particle size distribution analysis of sand-sized particles by laser diffraction: an experimental investigation of instrument sensitivity and the effects of particle shape. *Sedimentology* 53, 671-685.
- Bouma, A.H., 1962. *Sedimentology of some Flysch Deposits*, Elsevier, Amsterdam, 168 pp.
- d'Alessio M.A., Johansen I.A., Bürgmann R., Schmidt, D.A. Murray M. H., 2005. Slicing up the San Francisco Bay Area: block kinematics and fault slip rates from GPS-derived surface velocities. *Journal of Geophysical Research* 110, B06403, doi: 10.1029/2004JB003496.
- Darienzo, M.E., Peterson, C.D., 1990. Episodic tectonic subsidence of late Holocene salt marshes, northern Oregon central Cascadia margin. *Tectonics* 9, 1-22.
- Duncan, J.R., Fowler, G.A., Kulm, L.D., 1970. Planktonic Foraminiferan-Radiolarian ratios and Holocene-Late Pleistocene deep-sea stratigraphy off Oregon. *Geological Society of America Bulletin* 81, 561-566.
- Goldfinger, C., Morey, A., Erhardt, M., Nelson, C.H., Gutiérrez-Pastor, J., Enkin, R., Dallimore, A. 2006. Cascadia Great Earthquake Recurrence: Rupture Lengths, Correlations and Constrained OxCal Analysis of Event Ages. *Proceedings of the USGS Tsunami Sources*

- Workshop, Diggles, J., Geist, E., and Lee, H., eds. CD-ROM, April 21 and 22, 2006.
- Goldfinger, C., Grijalva, K., Bürgmann, R., Morey, A.E., Johnson, J.E., Nelson, C.H., Gutiérrez-Pastor, J., Ericsson, A., Karabanov, E., Chaytor, J.D., Patton, J., Gràcia, E., 2008. Late Holocene Rupture of the Northern San Andreas Fault and Possible Stress Linkage to the Cascadia Subduction Zone. *Earth Bulletin of the Seismological Society of America* 98, (2), 861-889.
- Goldfinger, C., Morey, A., Nelson, C.H., Gutierrez-Pastor, J., Johnson, J.E., Karabanov, E., Chaytor, J., the Shipboard Scientific Party, 2007. Rupture Lengths and Temporal History of Significant Earthquakes on the Offshore and North coast Segments of the Northern San Andreas. *Earth Planetary Science Letters* 254, 9-27.
- Goldfinger, C., Nelson, C.H., Johnson, J., 2003a. Holocene Earthquake Records From the Cascadia Subduction Zone and Northern San Andreas Fault Based on Precise Dating of Offshore Turbidites. *Annual Reviews of Geophysics* 31, 555-577.
- Goldfinger, C., Nelson, C.H., Johnson, J.E., 2003b. Deep-Water Turbidites as Holocene Earthquake Proxies: The Cascadia Subduction Zone and Northern San Andreas Fault Systems. *Annali Geofisica* 46, 1169-1194.
- Goldfinger, C., Nelson, C.H., Morey, A.E., Johnson, J.E., Patton, J., Karabanov, E., Gutiérrez-Pastor, J., Eriksson, A.T., Gràcia, E., Dunhill, G., Enkin, R.J., Dallimore, A., Vallier, T., 2012. Turbidite event history—Methods and implications for Holocene paleoseismicity of the Cascadia subduction zone: U.S. Geological Survey Professional Paper 1661–F, 184 p., available free at <http://pubs.usgs.gov/pp/pp1661f/>.
- Gorsline, D.S., De Diego, T., Nava-Sanchez, E.H., 2000. Seismically triggered turbidites in small margin basins: Alfonso Basin, Western Gulf of California and Santa Monica Basin, California Borderland. *Sedimentary Geology* 135, 21-35.
- Griggs, G.B., 1969, Cascadia Channel: The anatomy of a deep sea channel:, Oregon State University, Corvallis, Oregon, Unpublished Ph.D. Dissertation , pp.183.
- Gutierrez-Pastor J., Nelson, C.H., Goldfinger,C., Johnson, J.E., Escutia, C., Eriksson, A., Morey , A.E., the Shipboard Scientific Party, 2009. Earthquake Control of Holocene

- Turbidite Frequency confirmed by Hemipelagic Sedimentation Chronology on the Cascadia and Northern California Active Continental Margin, in: Kneller, B., McCaffrey, W., Martinsen, O.J. (Eds.), *External Controls on Deepwater Depositional Systems*, SEPM Special Publication 92, pp. 179-197.
- Kane, I., Hodgson, D.M., 2011. Submarine channel levees: nomenclature and criteria to differentiate subenvironments. Exhumed examples from the Rosario Fm. (Upper Cretaceous) of Baja California, Mexico, and the Laingsburg Fm. (Permian), Karoo Basin, S.Africa. *Marine and Petroleum Geology* 28, 807-823.
- Kelsey, H.M., Witter, R.C., Hemphill-Haley, E., 2002. Plate-boundary earthquakes and tsunamis of the past 5500 yr, Sixes River estuary, southern Oregon. *Geological Society of America Bulletin* 114 (3), 298-314.
- Kelson, K., Strieg, A., Koehler, R., Kang, K., 2006. Timing of Late Holocene Paleearthquakes on the Northern San Andreas Fault at the Fort Ross Orchard Site, Sonoma County, California. *Bulletin of the Seismological Society of America* 96 (3), 1012-1028.
- Kneller, B.C. and McCaffrey, W.D., 2003. The interpretation of vertical sequences in turbidite beds: The influence of longitudinal flow structure. *Journal of Sedimentary Research* 73, 706-713.
- Knudsen, K.L., Witter, R.C., Garrison-Laney, C.E., Baldwin, J.N., Carver, G.A., 2002. Past Earthquake-Induced Rapid Subsidence along the Northern San Andreas Fault: A New Paleoseismological Method for Investigating Strike-Slip Faults. *Bulletin of the Seismological Society of America* 92 (7), 2612-2636.
- Malinverno, A., Ryan, W.B.F., 1988. Sonar images of the path of recent failure events on the continental margin off Nice, France: in Clifton, H.E., ed., *Sedimentologic consequences of convulsive geologic events*. Geological Society of America, Special Paper 229, 59-75.
- Mulder, T., Syvitski, J.P. M., Migeon, S., Faugeres, J.C., Savoye, B., 2003. Marine hyperpycnal flows; initiation, behavior and related deposits, in: *Marine and Petroleum Geology, Turbidites: Models and Problems* 20, 861-882.

- Nakajima, T., Kanai, Y., 2000. Sedimentary features of seismoturbidites triggered by the 1983 and older historical earthquakes in the eastern margin of the Japan Sea. *Sedimentary Geology* 135, 1-19.
- Nelson, A.R., Atwater, B.F., Brobowski, P.T., Bradley, L.A., Clague, J.J., Carver, G.A., Darienzo, M.E., Grant, W.C., Krueger, H.W., Sparks, R., Stafford, T.W., Stuiver, M., 1995. Radiocarbon evidence for extensive plate-boundary rupture about 300 years ago at the Cascadia subduction zone. *Nature* 378, 371-374.
- Nelson, C.H., 1968. Marine Geology of Astoria Deep-Sea Fan: Oregon State University, Corvallis, Unpublished Ph.D. Dissertation, pp. 289.
- Nelson, C.H., 1976. Late Pleistocene and Holocene depositional trends, processes, and history of Astoria Deep-Sea Fan, northeast Pacific. *Marine Geology* 20, 129-173.
- Nelson, C.H., Escutia, C., Goldfinger, C. Karabanov, E., Gutiérrez-Pastor, J., 2009. External Controls on modern Clastic Turbidite Systems: Three Case Studies, in: Kneller, B., McCaffrey, W., Martinsen, O.J. (Eds.), *External Controls on Deepwater Depositional Systems*, SEPM Special. Publication 92, pp. 57-76.
- Nelson, C. H., Escutia, C., Goldfinger, C., Twichell, D.C., Damuth, J.E., 2011. Case Studies Comparing Mass-Transport and Turbidite-System Deposits in Different Continental Margin Settings and Time Periods, in: Shipp C., Weimer P., Posimentier, H., (Eds.), *Mass Transport Deposits*, SEPM Special Publication 95, pp. 39-66.
- Nelson, C.H., Goldfinger, C., Johnson, J.E., Dunhill, G., 2000. Variation of Modern Turbidite Systems Along the Subduction Zone Margin of Cascadia Basin and Implications for Turbidite Reservoir Beds, in: Weimer, P.W., Nelson, C.H. et al., (Eds.), *Deep-water Reservoirs of the World*, Gulf Coast Section Society of Economic Paleontologists and Mineralogists Foundation, 20 Annual Research Conference, p.714-7.
- Nelson, C.H., Karabanov, E.B., Colman, S.M., 1995. Late Quaternary Lake Baikal turbidite systems, Russia, in: Pickering, K.T., Lucchi, F.R., Smith, R., Hiscott, R.N., Kenyon, N. (Eds.), *An Atlas of Deep-Water Environments*, Chapman and Hall, London, pp. 29-33.
- Nelson, C.H., Maldonado, A., 1988. Factors controlling depositional patterns of Ebro turbidite

- systems, Mediterranean Sea. *American Association of Petroleum Geologists Bulletin* 72 (6), 698-716.
- Nelson, C.H., Maldonado, A., Barber, J.H., Alonso, B., 1992. Modern sand-rich and mud-rich silic-clastic aprons, alternative base-of-slope turbidite systems to submarine fans, in: Weimer, P., Link, M.H. (Eds.), *Seismic facies and sedimentary processes of modern and ancient submarine fans*. Springer-Verlog, New York, pp. 171-190.
- Niemi, T.M., Hall, N.T., 1992. Late Holocene slip rate and recurrence of great earthquakes on the San Andreas Fault in northern California. *Geology* 20, 195-198.
- Piper, D.J.W., Cochonat, P., Morrison, M., 1999. The sequence of events around the epicentre of the 1929 Grand Banks earthquake: initiation of debris flows and turbidity current inferred from sidescan sonar. *Sedimentology* 46, 79-97.
- Piper, D.J.W., Deptuck, M., 1997. Fine-grained turbidites of the Amazon Fan: facies characterization and interpretation. In R.D. Flood, D.J.W. Piper, A. Klaus, and L.C. Peterson (Eds.), *1997 Proceedings of the Ocean Drilling Program, Scientific Results* 155, 79-108.
- Prentice, C.S., Merritts, D.J., Beutner, E.C., Bodin, P., Schill, A., Muller, J.R., 1999. Northern San Andreas fault near Shelter Cove, California. *Geological Society of America Bulletin* 111, 512-523.
- Satake, K., Shimazaki, K., Tsuji, Y., Ueda, K., 1996. Time and size of a giant earthquake in Cascadia inferred from Japanese tsunami records of January, 1700. *Nature* 379, 246-249.
- Satake, K., Wang, K., Atwater, B.F., 2003. Fault slip and seismic moment of the 1700 Cascadia earthquake inferred from Japanese tsunami descriptions. *Journal of Geophysical Research*, B, Solid Earth and Planets 108, p. ESE 7-1.
- Schwartz, D.P., Pantosti, D., Okumura, K., Powers, T.J., Hamilton, J.C., 1998. Paleoseismic investigations in the Santa Cruz mountains, California: Implications for recurrence of large-magnitude earthquakes on the San Andreas Fault. *Journal of Geophysical Research* 103, p. 17,985-18,001.

- Segall, P., 2002, Integrating geologic and geodetic estimates of slip rate on the San Andreas fault system, *International Geology Review* 44 (1) 62-82.
- Shiki, T., Kumon, F., Inouchi, Y., Kontani, Y., Sakamoto, T., Tateishi, M., Matsubara, H., Fukuyama, K., 2000. Sedimentary features of the seismo-turbidites, Lake Biwa, Japan. *Sedimentary Geology* 135, 37-50.
- Sternberg, R.W., 1986. Transport and accumulation of river-derived sediment on the Washington continental shelf, USA. *Journal of Geological Society of London* 143, 945-956.
- Stow, D.A.V., Shanmugam, G., 1980. Sequence of structures in fine-grained turbidites: comparison of recent deep sea and ancient flysh sediments, *Sedimentary Geology*, 25, 23-42.
- Strasser, M., Anselmetti, F.S., Fäh, D., Giardini, D., Schnellmann, M., 2006. Magnitudes and source areas of large prehistoric northern Alpine earthquakes revealed by slope failures in lakes. *Geology* 8, 1005-1008.
- Tripsanas, E.K., Bryant, W.R., Slowey, N.C., Kim, J.W., 2006. Marine Isotope Stage 6 Canyon and Spillover Deposits of the Bryant and Eastern Canyon Systems, Northwest Gulf of Mexico: Importance of Fine-Grained Turbidites on a Delta-Fed Prograding Slope. *Journal of Sedimentary Research* 76 (8), 1012-1034.
- Twichell, D.C., Nelson, C.H., Damuth, J.E., Olson, H. C., Dun hill, G., 2000. Bryant Canyon Turbidite System Pathway on the Louisiana Continental Slope, Northern Gulf of Mexico. *Gulf Coast Association of Geological Societies Transactions* L.
- Twichell, D.C., Nelson, C.H., Kenyon, N.H., Schwab, W.C., 2009. The influence of external processes on the Holocene evolution of Mississippi fan, in: Kneller, B., McCaffrey, W., Martinsen, O.J. (Eds.), *External Controls on Deepwater Depositional Systems*, SEPM Special. Publication 92, pp. 145-157.
- Twichell, D.C., Schwab, W.C., Nelson, C.H., Lee, H.J., Kenyon, N.H., 1992. Characteristics of a sandy depositional lobe on the outer Mississippi Fan from Sea MARC IA sidescan sonar images. *Geology* 20, 689-692.
- Wolf, S.W., Hamer, M., 1999. Turbidite pathways in Cascadia Basin and Tufts abyssal plain;

Part A, Astoria Channel, Blanco Valley, and Gorda Basin. U.S.G.S. Open File Report OF 99-0157.

Zdanowicz, C.M., Zielinski, G.A., Germani, M.S., 1999. Mount Mazama eruption: calendrical age verified and atmospheric impact assessed. *Geology* 27, 621-624.

Zhang, H., Niemi, T., Fumal, T., 2006. A 3000-year Record of Earthquakes on the Northern San Andreas Fault at the Vedanta Marsh Site, Olema. *California Seismological Research Letters* 77 (2), 248.

FIGURE CAPTIONS

Figure 1. The Cascadia margin turbidite systems, core locations and the geological setting of the active tectonic continental margin associated with the Cascadia Subduction Zone made up of the Juan de Fuca and Gorda Plates (modified from Goldfinger et al., 2008).

Figure 2. Northern California margin turbidite systems, core locations and geological setting of the active tectonic margin associated with the northern San Andreas Fault.

Figure 3. Analysis of core sections. A) Definition of turbidite versus hemipelagic sediment sequences (modified from Gutierrez-Pastor et al., 2009). B) X-rays, physical properties, grain size samples and mineralogy of 24GC of the northern California margin (mineralogy from Goldfinger et al., 2007). C) Example of turbidite correlations in Juan de Fuca and Cascadia Channels margin based on lithology, physical properties and radiocarbon ages (modified from Gutierrez-Pastor et al., 2009).

Figure 4. Cascadia margin core sections of 12PC in Juan de Fuca Channel, 25 PC in Cascadia Channel and 14PC in Willapa Channel showing core photos, X-ray radiographs, grain size and physical properties (density and magnetic signatures) Characteristics of correlative turbidite T3 in Juan de Fuca and Cascadia Channels can be compared. Turbidites in the Willapa

Channel, another tributary of the Cascadia Channel, are examples of turbidites in a proximal channel at the base of the slope. Dots show grain size sample locations and large numbers besides the dots are the median grain size (d₅₀) in a phi (ϕ) scale for each sample. Numbers down the core sections identify the correlative turbidites.

Figure 5. Grain size distribution curves of turbidites from 25PC of Cascadia Channel.

Figure 6. Northern California margin core sections from 49 PC in Noyo Canyon, 13 PC in Gualala Canyon Head, 12PC in Gualala Channel, 24GC below Noyo/Gulala/Viscaino channel confluence and 31PC below Viscaino/Cordell channel confluence showing core photo and CT scan of 49PC, X-ray radiographs of other cores, physical properties (density and magnetic signatures) and grain size. Note that there is no available density signature for 24GC. Large dots are the grain size sample locations and large numbers besides the dots are the median grain size (d₅₀) for each sample. Small dots show mineralogic sample locations.

Figure 7. Grain size distribution curves of turbidites from 24GC below Noyo/Gualala/Viscaino Channel confluence.

Figure 8. Number of pulses of correlative turbidites at sites in Juan de Fuca and Cascadia Channels (data sources from Figs. 3C and 4; Goldfinger et al., 2003a; 2003b; 2008; Gutierrez-Pastor et al., 2009, Goldfinger et al., 2012). Goldfinger et al., (2012) show that there is a 0.96 confidence in the Pearson correlatin matrix of pulses in correlative turbidites from different Cascadia Basin turbidite systems.

Figure 9. Number of pulses per turbidite in Noyo Channel of the northern California margin based on physical properties and lithology (modified from Goldfinger et al., 2007). Note that we have interpreted the density signature as the most reliable proxy of grain size.

Figure 10. A) Morphologic model for seismo-turbidite deposition in the active tectonic margins of western North America. Uni-pulsed, multi-pulsed or stacked turbidites are correlated with each type of canyon or channel morphologic setting and magnitude of the earthquake. B) Location of sample sites in the channel systems of Cascadia and northern California margins. Numbers in part B correspond to the numbers in the morphologic model settings of part A.

Table 1A. Thickness and features of turbidites in Cascadia margin sites.

Table 1B. Grain size analysis of Cascadia margin turbidites. The grain size is in a phi (ϕ) scale ($\phi = \log_2 \text{ mm}$) with the lower values corresponding to the coarser grain size of the sediments (1-4 ϕ = sand, 4-8 ϕ = silt and 8-10 ϕ = clay). In table 1A the key percentiles (d50 and d90) of each curve and the % volume of sand, silt and clay are shown. D50 is the median grain size for each sample and D90 is the maximum grain size for each sample.

Table 2A. Thickness and features of turbidites at northern California margin sites.

Table 2B. Grain size analysis of northern California margin turbidites. The grain size is in a phi (ϕ) scale ($\phi = \log_2 \text{ mm}$) with the lower values corresponding to the coarser grain size of the sediments (1-4 ϕ = sand, 4-8 ϕ = silt and 8-10 ϕ = clay). In table 2A the key percentiles (d50 and d90) of each curve and the % volume of sand, silt and clay are shown. D50 is the median grain size for each sample and D90 is the maximum grain size for each sample.

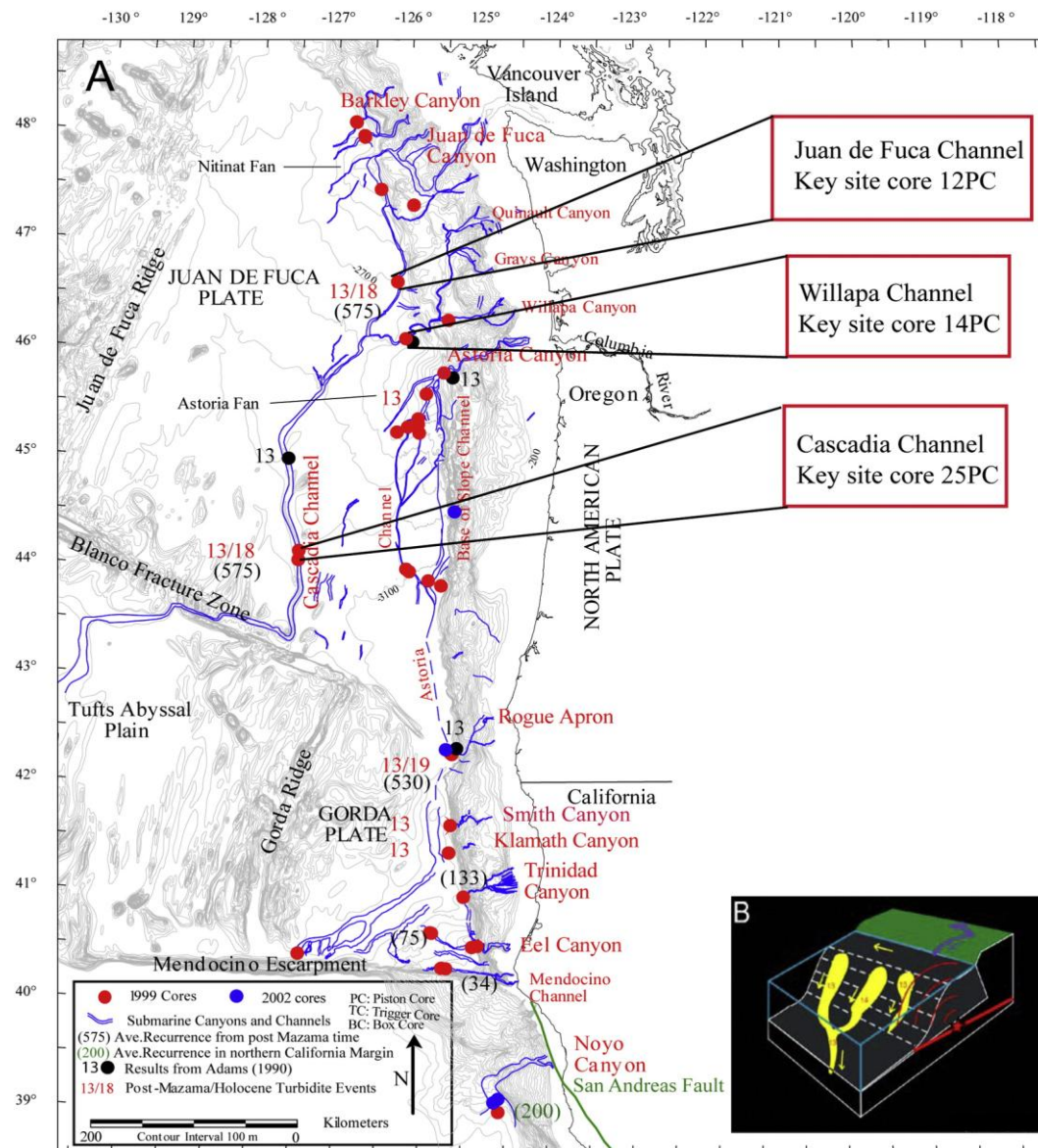


Figure 1

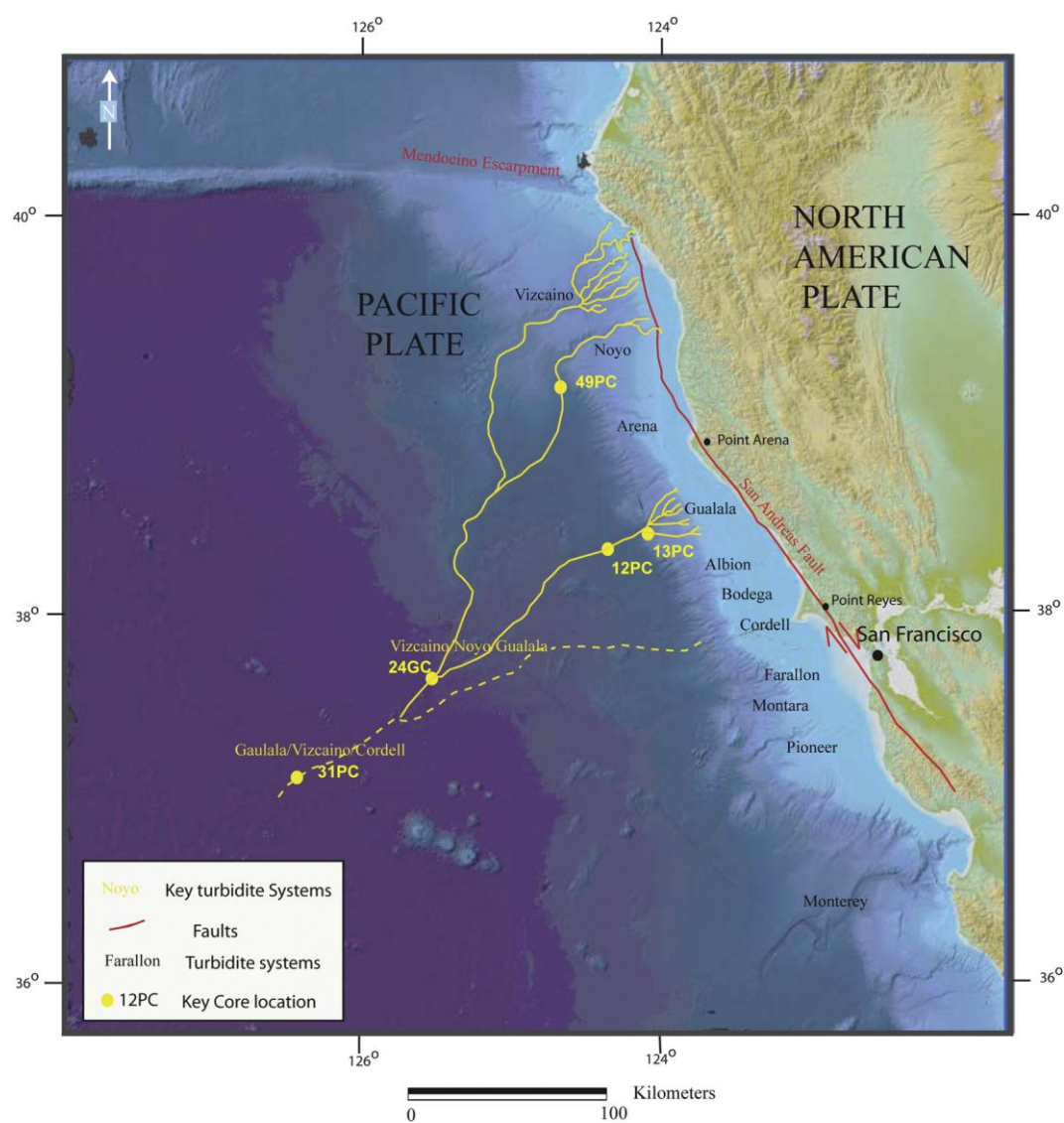


Figure 2

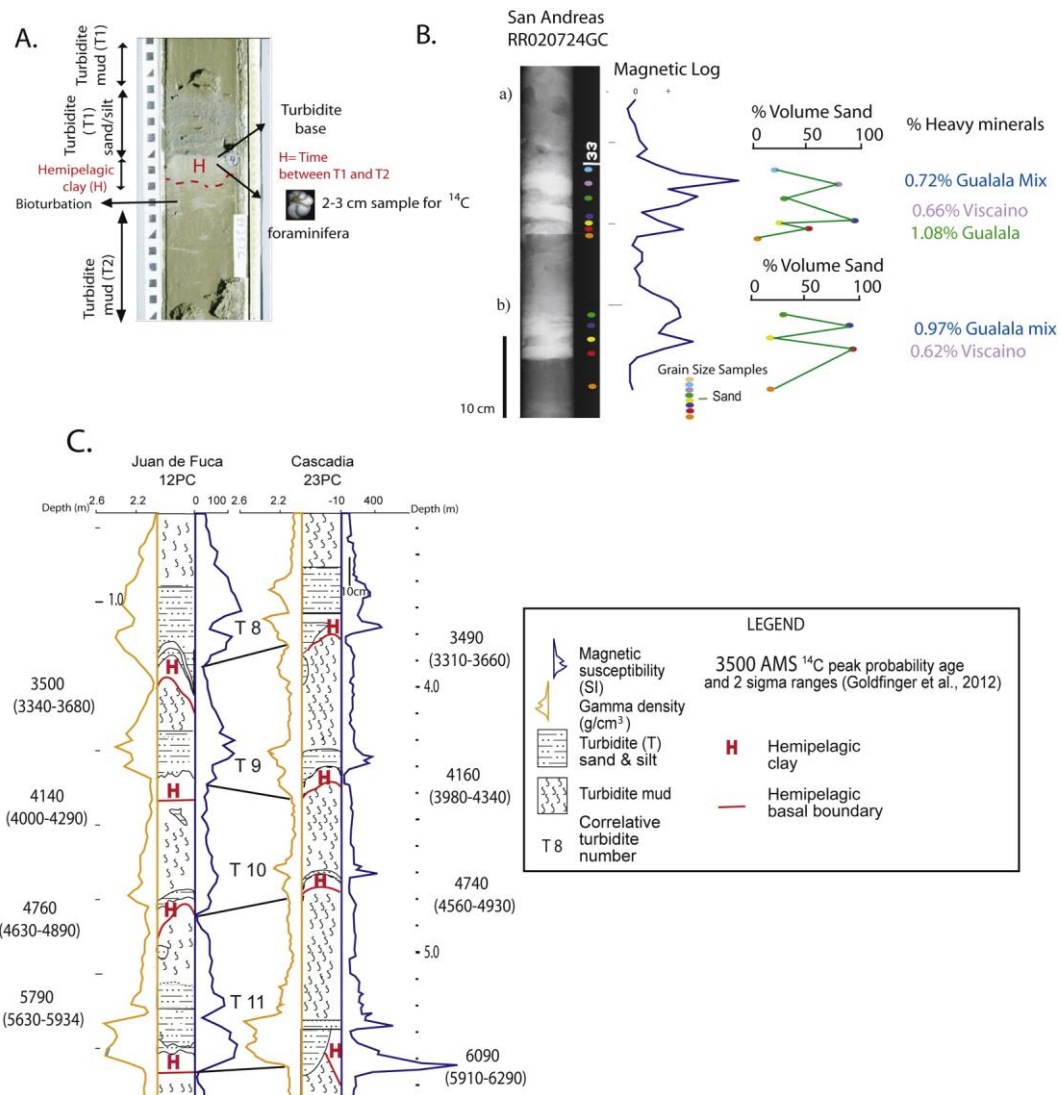


Figure 3

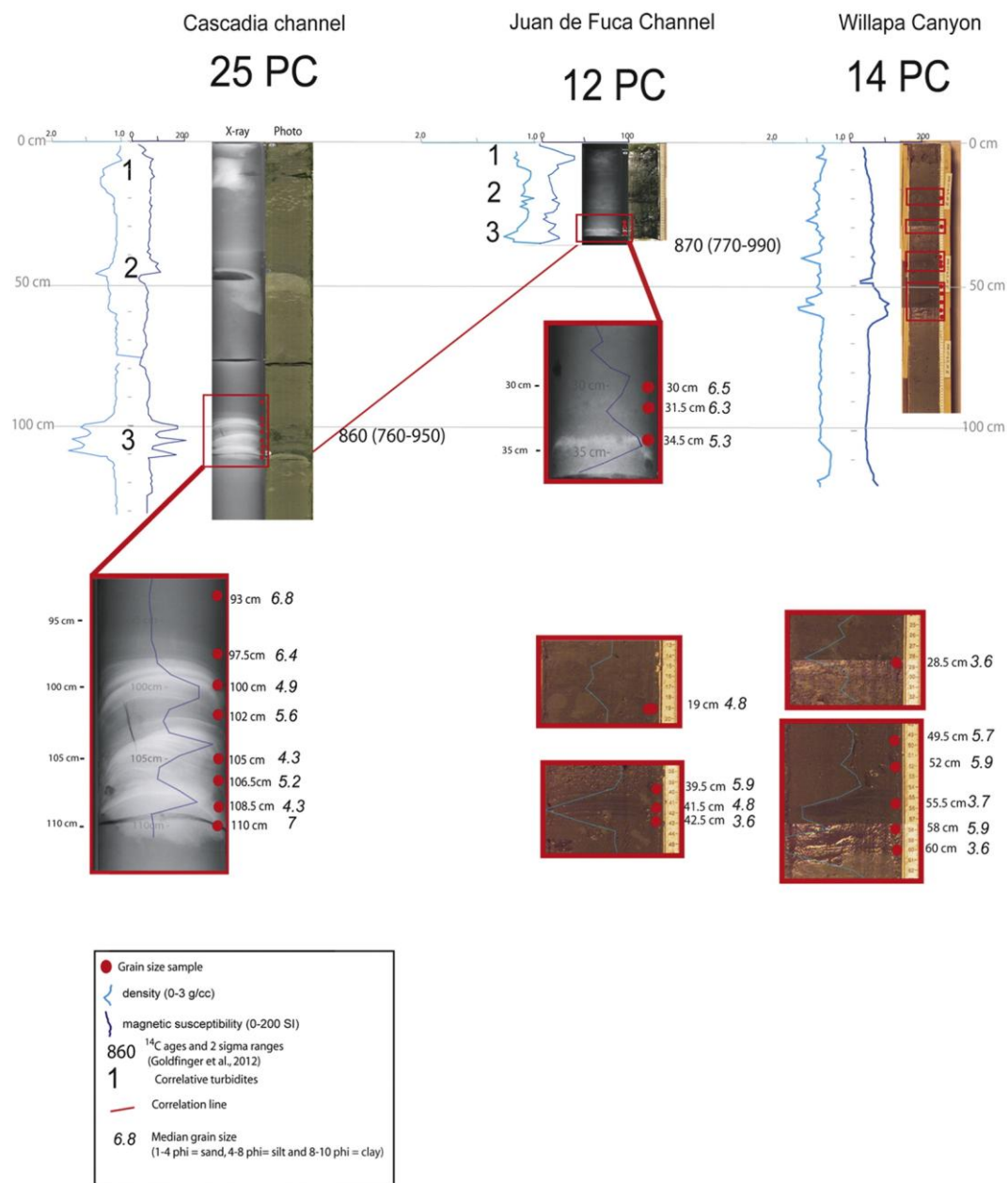


Figure 4

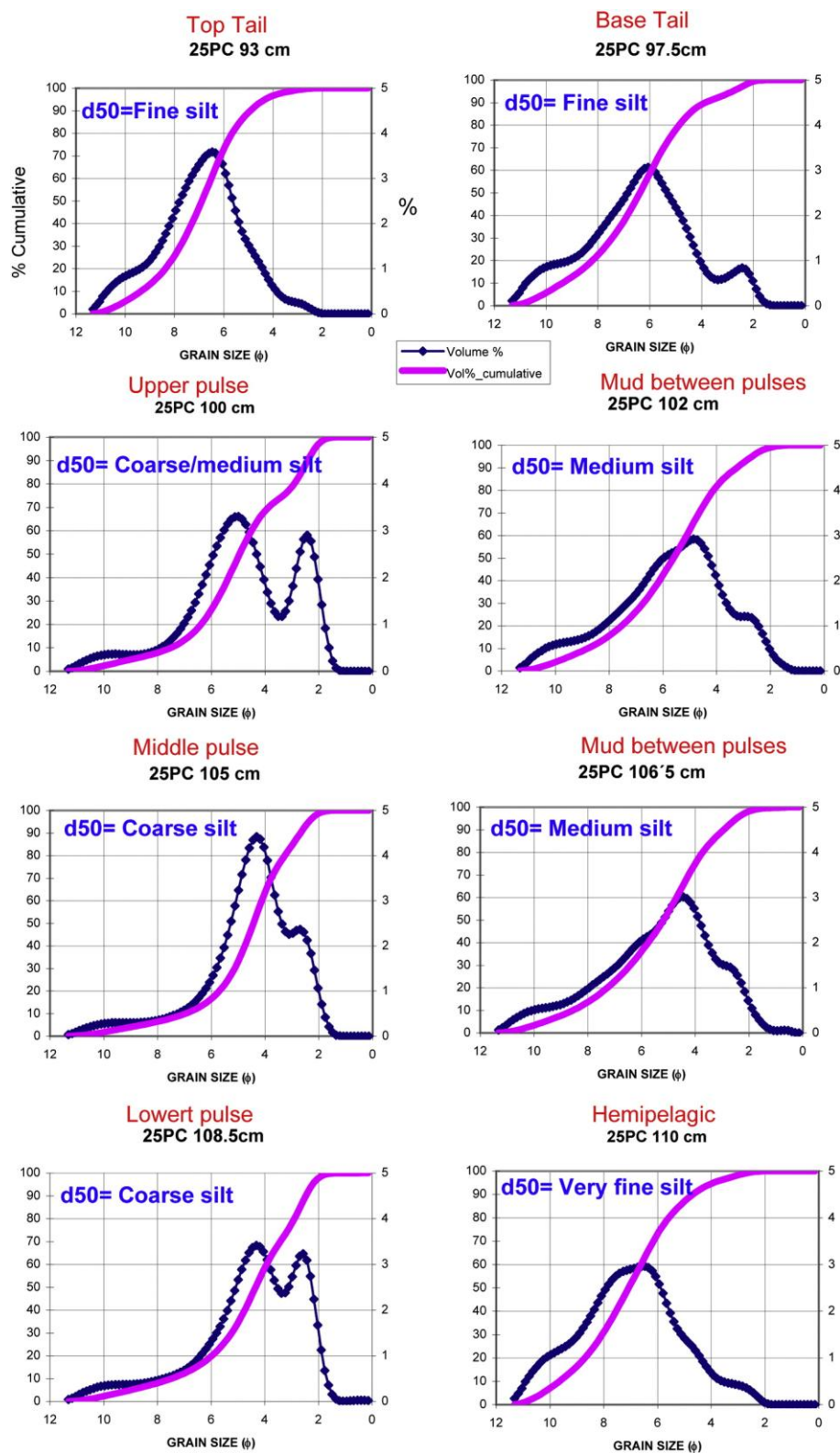


Figure 5

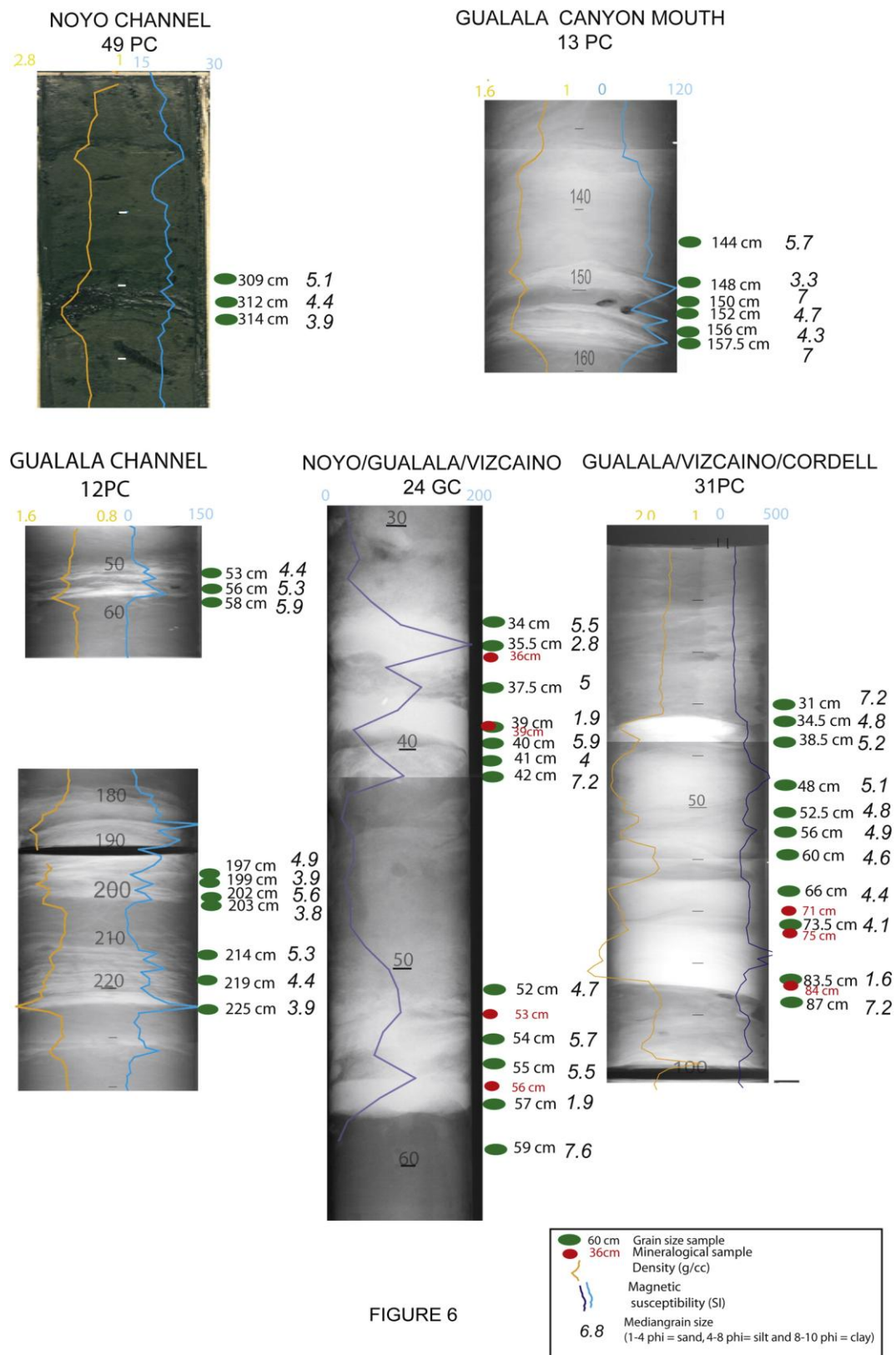


Figure 6

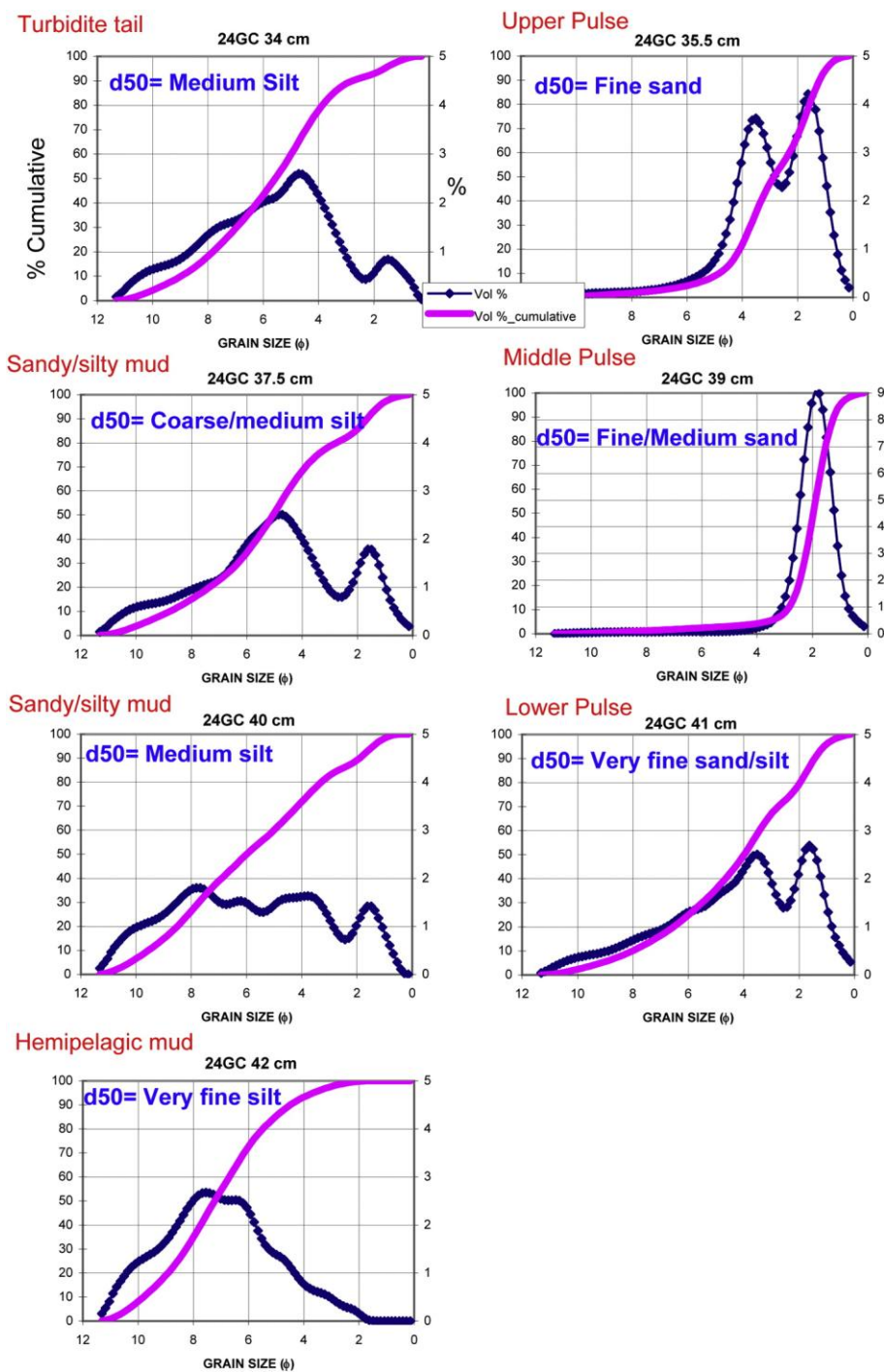


Figure 7

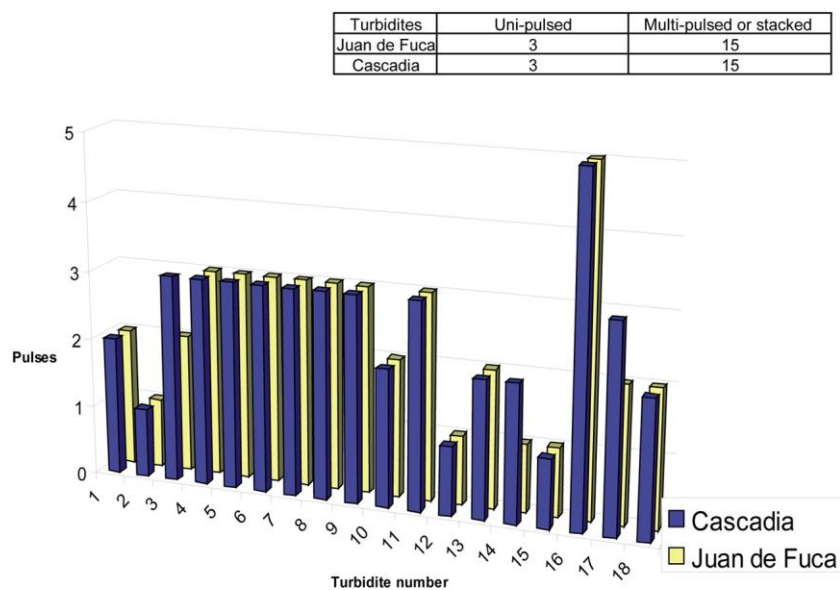


Figure 8

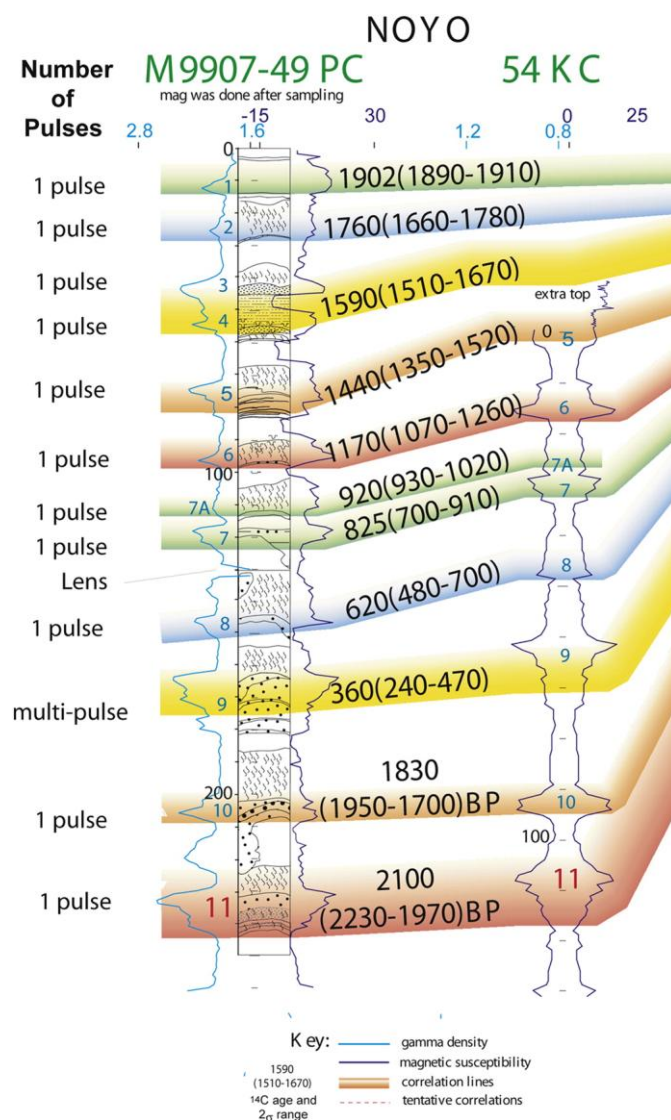


Figure 9

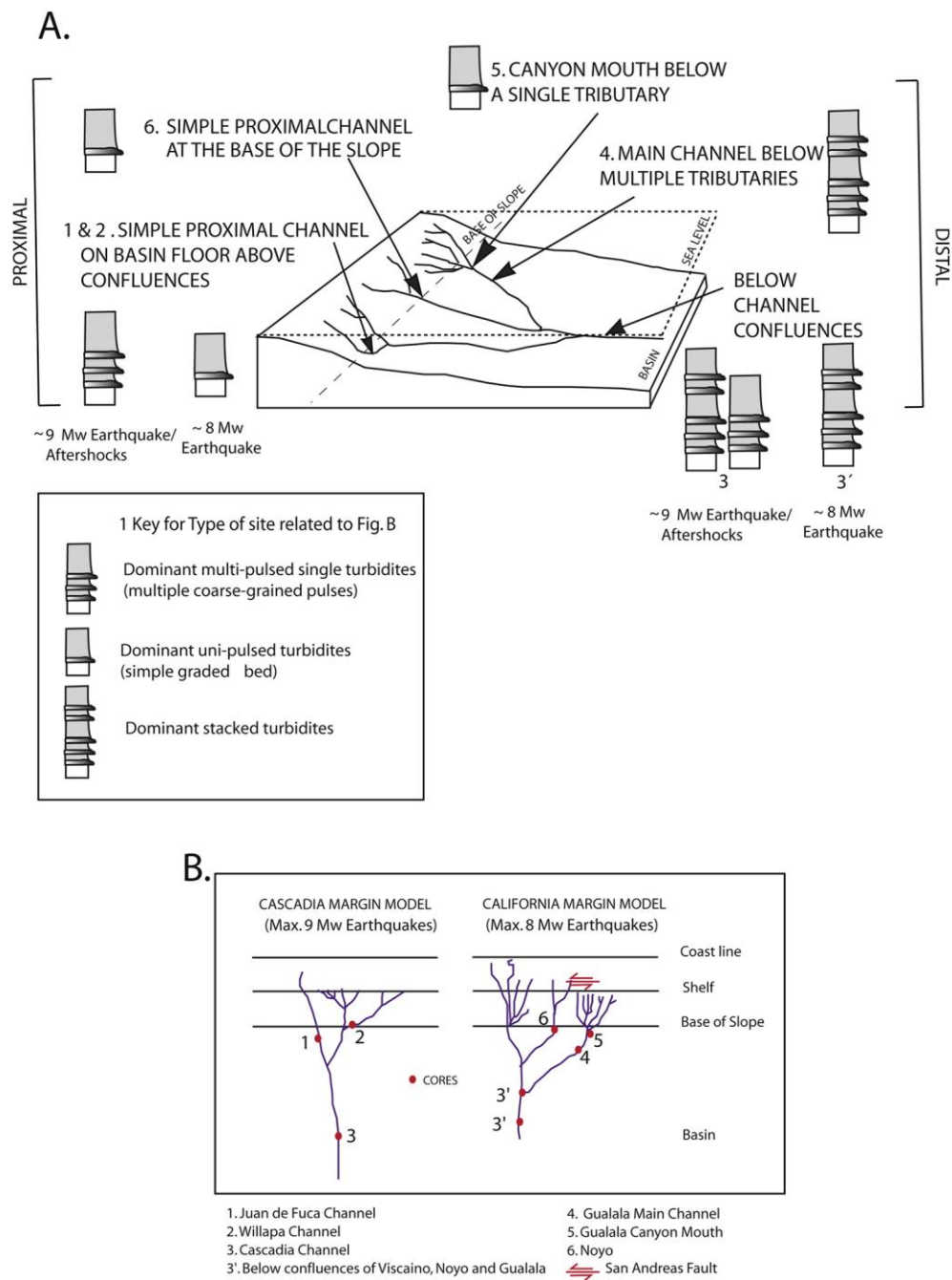


Figure 10

TABLE 1.A

GRAIN SIZE ANALYSIS

Samples	Turbidite	Tail	Hemipelagic	Base	Structures	Pulses	Sequences
Juan de Fuca 12 PC	9 cm	5 cm	5 cm		not identified	1	fining upward
Cascadia 25 PC	12 cm	45 cm	1 cm	sharp, erosive	lamination, ripples	3	truncated Bouma
Willapa 14PC at 60cm	11 cm	7 cm	46 cm	erosive	not identified	2	no sequence
at 42 cm	3 cm	10 cm	not distinguished		lamination	1	fining upward
at 28.5 cm	0.5 cm?	?	not distinguished	?	?	1	no sequence
at 19 cm	0.5 cm?	?	not distinguished	?	?	1	no sequence

TABLE 1.B

T3 Sample Depth	d50 (φ)	d90 (φ)	% Sand	% Silt	% Clay	Interpretation (Sediment structures and grain size)
Juan de Fuca 12 PC	34.5 cm 31.5 cm 30 cm	5.3 6.3 6.5	3.3 3.2 3.9	21 15 10	63 64 66	16 21 24
	110 cm	7	4.5	6	65	29
	108.5 cm	4.3	2.4	43	49	8
	106.5 cm	5.2	2.9	26	61	13
	105 cm	4.3	2.3	38	56	6
Cascadia 25 PC	102 cm	5.6	3.2	19	66	15
	100 cm	4.9	2.4	19	66	15
	97.5 cm	6.4	3.7	11	67	22
	93 cm	6.8	4.8	4	72	24
	60 cm	3.6	2.2	54	35	11
	58 cm	5.9	2.7	29	54	17
	55.5 cm	3.7	2.4	55	35	10
	52 cm	5.9	2.8	30	52	18
Willapa 14PC	49.5 cm	5.7	2.9	30	52	18
	42.5 cm	3.6	2.5	59	31	10
	41.5 cm	4.8	2.7	41	44	15
	39.5 cm	5.9	2.3	27	54	19
	28.5 cm	3.6	2.8	66	29	5
	19 cm	4.8	2.8	38	47	15

d50 is the median , showing the most representative grain size in the sample

d90 is the coarsest grain size in the sample

T Turbidite

TABLE 2.A

Samples	Turbidite	Tail	Hemipelagic	Base	Structures	Pulses	Sequences
Noyo							
49PC	5 cm	12 cm	6 cm	sharp	no identified	1	fining upward
Gualala							
13PC							
at 157 cm	6 cm	not distinguished	10 cm?	sharp	lamination	1	fining upward
at 150 cm	2 cm	8 cm?	2 cm	sharp	lamination	1	
12PC							
at 58 cm	8 cm	51 cm?	12cm?		lenses	2 or 3	coarsing upward
at 203 cm	23 cm	40 cm	5 cm	erosional	lamination, ripples, lenses	4	amalgamation, pulses
at 225 cm	13 cm	3-4 cm	2-4cm	erosional	lamination	1	fining upward
24 GC							
at 42 cm	7 cm	22 cm	3 cm	sharp	no identified	3	pulses fining upward, overall coarsing upward
at 57.5 cm	7 cm	8.5 cm	4.5 cm	sharp	no identified	2	fining upward
31 PC							
at 85 cm	20 cm	?	5 cm?	erosional	lamination	2	fining upward
at 60 cm	28 cm	32 cm	5 cm?	erosional	lamination	3	fining upward

TABLE 2 B	Sample Depth	d50 (φ)	d90 (φ)	% Sand	% Silt	% Clay	Interpretation (Sediment structures and grain size)
Noyo 49 PC	314 cm	3,9	3,2	35	53	12	Tb ?
	312 cm	4,4	3,2	36	49	15	Tb ?
	309 cm	5,1	3,3	20	64	16	Tb or Tc?
Gualala 13PC	157.5 cm	7	4	8	61	31	Hemipelagic
	156 cm	4,3	3,1	42	45	13	Tb or Tc
	152 cm	4,7	3,2	37	46	17	Tb or Tc
	150 cm	7	4,3	6	62	32	Hemipelagic
	148 cm	3,3	3,3	33	55	12	Tb
	144 cm	5,7	2,4	28	53	19	mud, fecal pellets, bi-modal
Gualala 12 PC	225 cm	3,9	3	57	36	7	Tb, less clay, less silt
	219 cm	4,4	3,1	40	46	14	Tb
	214c cm	5,3	3,2	25	58	17	Tb, more clay, more silt
	203 cm	3,8	3	56	33	18	Tb or Tc
	202 cm	5,6	2,9	33	48	10	Bi-modal, Tc
	199 cm	3,9	3	55	35	19	Tb or Tc
	197 cm	4,9	3,1	37	45	11	Bi-modal, Tc
	58 cm	5,9	3,2	23	55	22	sandy /silty lense, high clay content
Noyo/Gualala/ Viscaino 24GC	56 cm	5,3	3,3	23	60	17	sandy /silty lense
	53 cm	4,4	3,7	33	59	8	sandy /silty lense, low clay content
	59 cm	7,6	4,4	7	52	41	mud with the lowest sand content
	57 cm	1,9	1,2	95	3	2	Ta
	55 cm	5,5	2,1	22	61	17	mud
	54 cm	5,7	1,2	91	8	1	Ta
	52 cm	4,7	2,5	35	53	12	mud with the highest sand content
	42 cm	7,2	4,4	7	60	33	mud, hemipelagic
	41 cm	4	1,4	51	39	10	Tc or Tb, bi-modal
	40 cm	5,9	1,8	29	46	25	mud
	39 cm	1,9	1,2	96	3	1	Ta
	37.5 cm	5	1,6	32	53	14	mud? High sand content , between pulses
	35.5 cm	2,8	1,2	79	19	2	Tb
	34 cm	5,5	1,5	23	60	17	Te, mud
	87 cm	7,2	4,4	7	60	33	silty mud
	83.5 cm	1,6	0,5	94	5	1	Ta, high sand %
	73.5 cm	4,1	2,8	45	48	7	mud
Viscaino/ Cordell 31 PC	66 cm	4,4	3,5	29	67	4	silty bed
	60 cm	4,6	2,8	34	53	13	Tc?, more and coarser sand
	56 cm	4,9	4	10	85	5	Tc?
	52.5 cm	4,8	3,3	25	65	10	Tc?, more and coarser sand
	48 cm	5,1	4,1	7	87	6	silt, Td?
	38.5 cm	5,2	3,3	22	62	16	silty bed between pulses
	34.5 cm	4,8	3,6	20	73	7	silty bed
	31 cm	7,2	4,4	6	60	34	mud, tail

Highlights

- Characteristics of Holocene seismo-turbidites from NW American active tectonic margins.
- Shaking signatures of ~ 9 Mw earthquakes cause individual multi-pulsed turbidites.
- 8Mw earthquakes plus downstream tributary canyon/channel confluences cause stacked turbidites.